Sixth Month Progess Report for the Period Aug. 15, 1987 - Feb. 14, 1988

on

Computer-Aided Modeling and Prediction of Performance of the Modified Lundell Class of Alternators in Space Station Solar Dynamic Power Systems

Grant No. NAG3 - 818

by

Nabeel A. O. Demerdash

Principal Investigator

and

Ren-hong Wang

Research Assistant

Department of Electrical and Computer Engineering

Clarkson University

Potsdam, New York, March 15, 1988

Submitted to

Solar Dynamic Module Division

Mail Stop 500 - 316

NASA Lewis Research Center

21000 Brookpark Road

Cleveland, Ohio 44135

Sixth Month Process Report for the Period Aug. 15, 1987 - Feb. 14, 1988

on

Computer-Aided Modeling and Prediction of Performance of the Modified Lundell Class of Alternators in Space Station Solar Dynamic Power Systems

by

Nabeel A. O. Demerdash

Principal Investigator

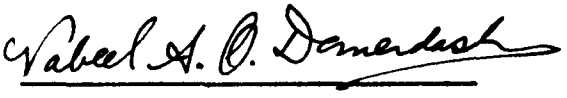

and

Ren-hong Wang

Research Assistant

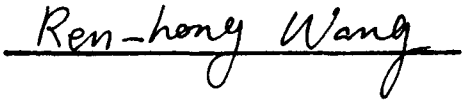

Department of Electrical and Computer Engineering

Clarkson University

Potsdam, New York, March 15, 1988

TABLE OF CONTENTS

1.0 Introduction

2.0 Nature of the Geometry of the Modified Lundell Class of Alternators

3.0 Basic Building Blocks and Nature of the Finite Element Grids

3.1 Tetrahedral Finite Elements

3.2 Triangular Prism Super-Elements

3.3 Filling Technique

4.0 Stator Finite Element Grid Geometry

4.1 Basic Grid Module for the Stator Grid

4.2 Stator Grid Presentation

4.3 Programming Considerations

5.0 Rotor Finite Element Grid Geometry

6.0 Immediate Forthcoming Efforts

7.0 Conclusions

8.0 References

1.0 INTRODUCTION

The main purpose of this project is the development of computer-aided models for purposes of studying the effects of various design changes on the parameters and performance characteristics of the Modified Lundell Class of Alternators (MLA), as components of a solar dynamic power system supplying electric energy needs in the forthcoming space station. Hence, this computer-aided modeling effort is expected to yield the tools necessary to assesses advantages and drawbacks of various proposed design variations (including material, geometric, and winding changes) on the basic design concept of the MLA class of alternators. This effort is expected to include the steady state as well as the dynamic performance characteristics of these types of high speed machines.

Key to this modeling effort is the computation of magnetic field distribution in this class of MLAs. Knowledge of such magnetic field distribution is the key element in finding the following: fluxes, induced emfs in various windings, winding inductances (reactances), various time constants and damping effects, critical effects of saturation on performance, critical areas of high magnetic and electric loading in various parts of such machines, amd hence loss distributions, efficiencies, dynamic characteristics and parameters, etc..

The nature of the magnetic field in this class of machines is unfortunately three-dimensional (3-D), and does not lend itself to reasonable two-dimensional (2-D) approximations. Accordingly, the magnetic field computation effort will entirely be based on the 3-D finite element (FE) method. In this method, one must discretize the solution volume, or region of interest, into small subdivisions called finite elements. The basic 3-D shaped discretization volume or element which will

be used in this investigation is the tetrahedron. The tetrahedral shape is the simplist, most general, and most flexible to use in a discretization process. Also, its finite element algebra is the most simple to develop. Hence, it possesses several attractive features from a numerical or computational standpoint. However, intermediate super-elements, such as triangular prisms and/or hexahedrons are resorted to in the development of the necessary finite element grids, for easier implementation and mental visualization of 3-D objects and parts.

Accordingly, in the early tasks of this investigation stator and rotor finite element grid discretizations for this class of MLAs are being developed. This effort was devided into stator and rotor grid discretizations, for purposes of being able to study the magnetic field distribution at various relative rotor to stator positions, as required by any rotating machinery modeling and analysis effort.

In this report, details of the development of the stator 3-D finite element grid are given. Also, a preliminary look at the early stage of 3-D FE rotor grid development effort is presented. In addition, a review of the immediately forthcoming tasks [1], based on the task flow chart, Figure 1.1, are discussed in the later portions of this report.

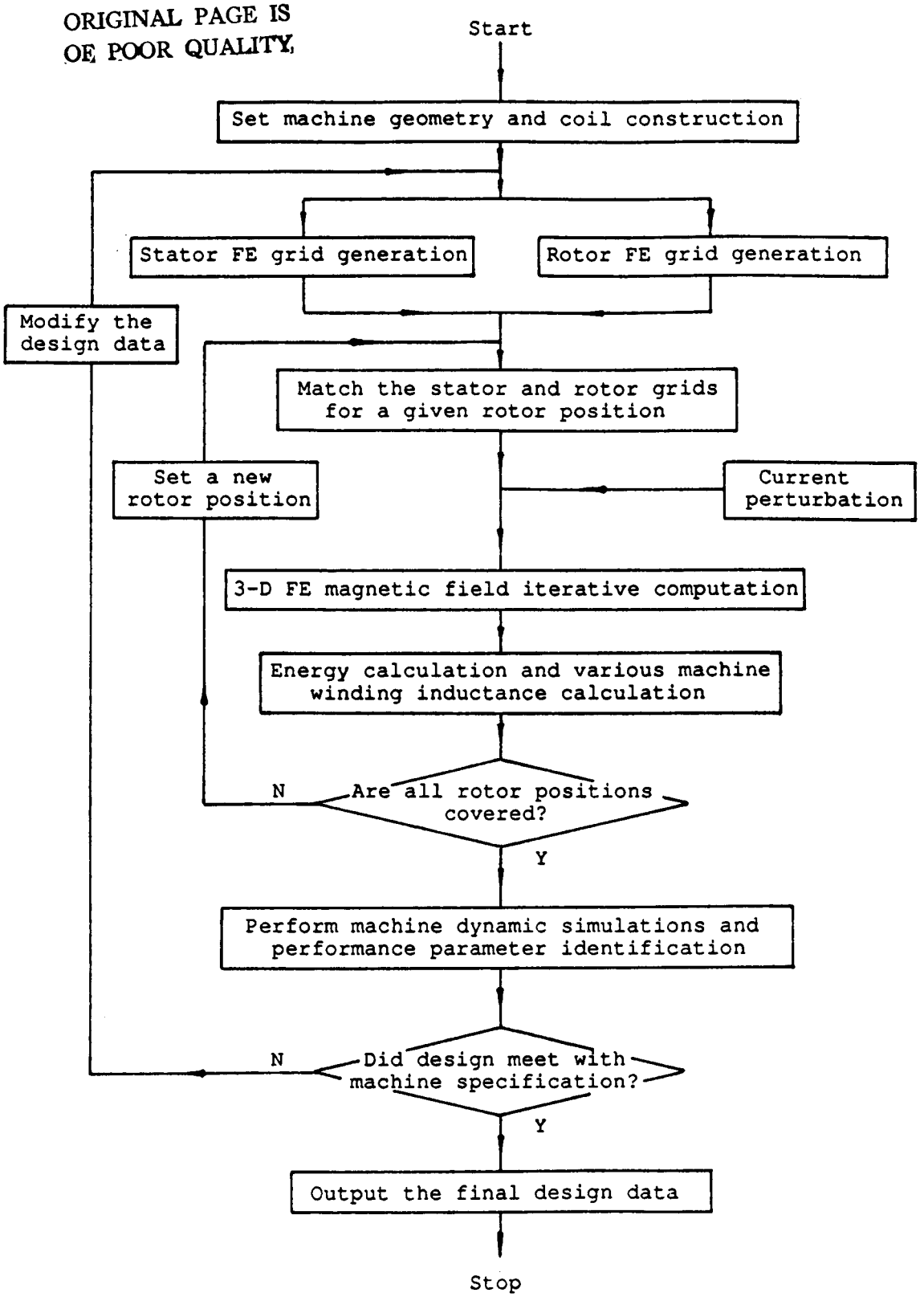

Figure 1.1 Flow Chart Outline of Investigation

2.0 NATURE OF THE GEOMETRY OF THE MODIFIED LUNDELL CLASS OF ALTERNATORS

The base example chosen for the current stage of this investigation is a 14.3 kVA, 1200 Hz Modified Lundell Alternator. This machine was developed for NASA Lewis Research Center for purposes of space power systems. The development of this machine by the AiResearch Manufacturing Company took place, in the 1960s. A very high rated speed, 36000 rpm, is the design key for the machine to reduce its volume and weight per voltampere to meet with the volume and weight limitation requirements in space applications. In this alternator, both the field excitation winding and the armature winding are stationary, and a mechanically strong, smooth rotor with special configuration is supported by gas bearings. The particular constructional feature of this MLA type of machine causes a different three dimensional pattern of magnetic flux paths inside the alternator, as compared with the predominantly two dimensional pattern of flux in ordinary synchronous machines. Accordinly, to calculate various winding inductances and performance parameters of this machine from magnetic field solutions, three dimensional magnetic field computations must be carried out through the machine geometry.

The basic configuration of this 14.3 kVA MLA with each major electric component identified, is illustrated in Figure 2.1, copied from Reference [2]. The stator contains a conventional three phase armature, as well as stationary field coils, which create the main magnetic flux in the axial direction of the machine. The rotor consists of two identical magnetic sections, as shown in Figure 2.2, also copied from Referenc [2]. Inserted between these two magnetic sections is a nonmagnetic separator. The rotor establishes four rotating magnetic poles when it carries magnetic

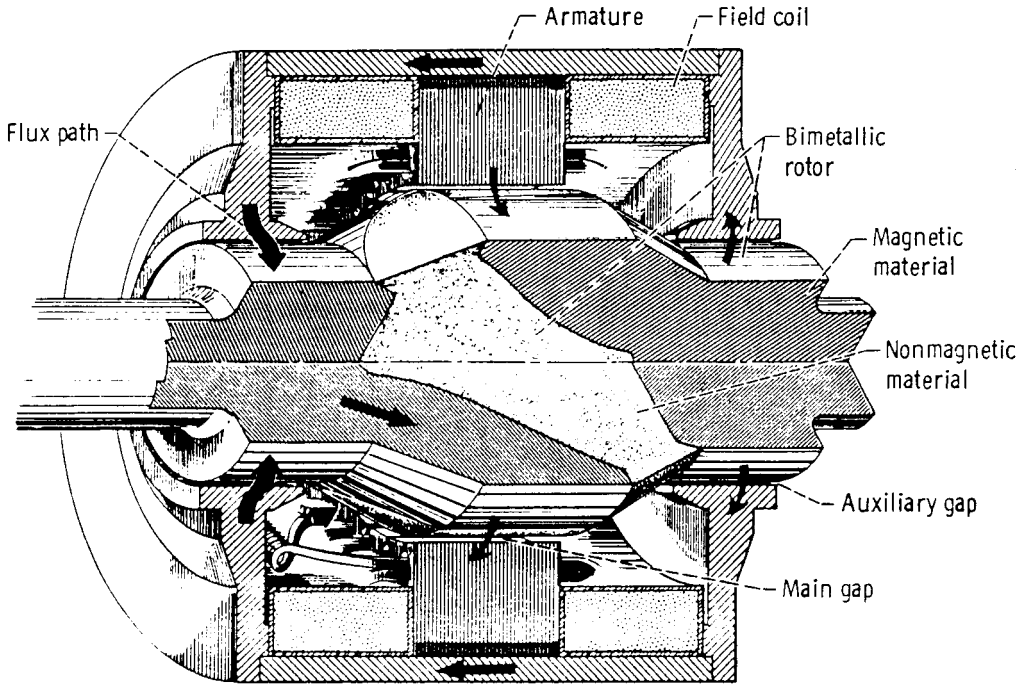

Figure 2.1 Cutaway View of the Modified Lundell Alternator

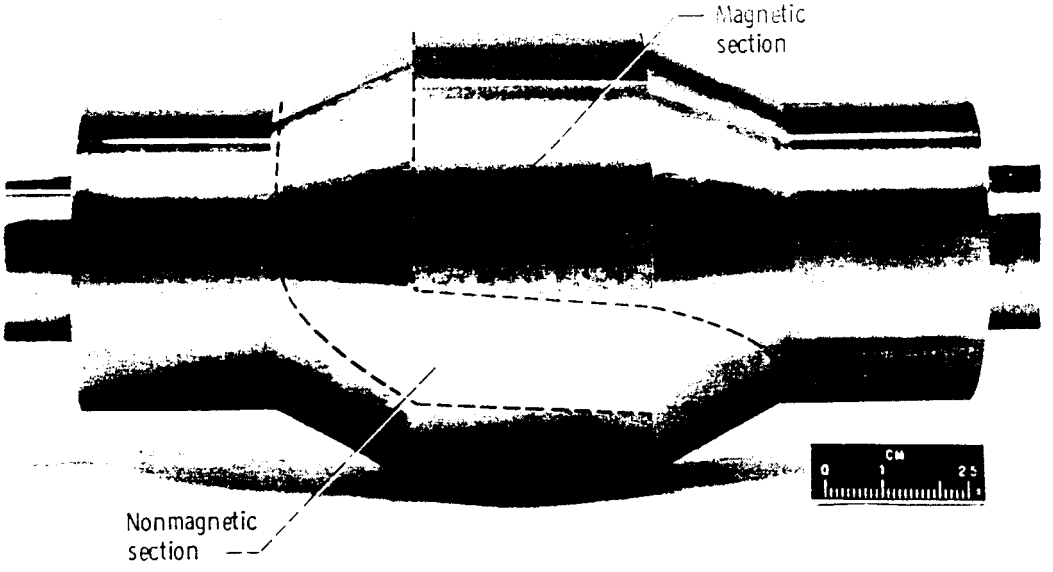

Figure 2.2 Rotor of Example 14.3 kVA MLA

flux and rotates. Also, the rotor carries portions of the axial paths which contribute to the overall values of the various machine winding inductances.

In Figure 2.1, the arrows are used to show the main magnetic flux path in the MLA machine. The flux starts from a north pole on the rotor, crosses the main airgap and proceeds radially through the stator teeth into the laminated stator core. It then goes circumferentially through the stator core for a distance of one pole pitch, enters the teeth radially and crosses the main airgap, in an opposite direction to the previous crossing, into the adjacent south poles on the rotor. The flux then goes axially down the rotor and crosses the first auxiliary air gap into the endbell and the outer frame. It leaves the other end of the frame , crosses the second auxiliary air gap, and completes its path back to the north pole from which it started. Such a picture of magnetic flux shows that the magnetic field inside the machine has not only radial and circumferential components in the stator laminations but also axial component in the rotor and the housing parts. Therefore, the magnetic field of the MLA machine has a true three dimensional nature. Accordingly, these investigators hold the view that no practical two dimensional approximation can be made to model such a magnetic field distribution, with a reasonably assured accuracy of results.

Accordingly, a three dimensional finite element vector potential solution model will be developed for the magnetic field calculation. As a first step in performing finite element calculations, three dimensional finite element grids which discretize the machine geometry into finite small sub-regions are generated. Detailed work of the generation of the finite element grids will be presented in Sections 3.0 through 5.0 of this report. It should be mentioned that the grid pictures shown later in this report are only for the example 14.3 kVA MLA machine. The computer pro-

gram developed for the grid generation has a capability to accommodate different machine design data and parameters for other cases, with variations in these parameters such as the key dimensions of the geometry, the number of poles, the armature coil pitch, the number of turns in various coils, coil dimensions, etc., within a practical range.

The key geometric dimensions of the cores, windings, etc., of the example machine are give in Table 2.1, and Figures 2.3 through 2.5. Such a machine geometry model is utilized here as the solution region for the three dimensional finite element calculations. The data in Table 2.1 with their corresponding definitions shown in Figures 2.3 through 2.5, are the input data for the computer algorithm which determines the topology of the finite element grid. As is shown by these figures, this machine geometry model closely duplicates the physical details of this MLA type of machine. Thus using this machine geometry model, magnetic field solutions can be expected to be close to the real magnetic field distribution of the actual machine.

It should be pointed out that a slight approximation was made in developing the machine geometry model presented above. Namely, that approximation is the fact that the model has not included ventilation tunnels inside the endbell and the frame of the machine. Meanwile, the axial thickness of the endbell and the outside diameter of the frame are modified to compensate for the geometry change due to this exclusion. Since the degree of magnetic saturation in the housing parts is usually a moderate one, such an approximation, if implemented carefully, will not affect the total magnetic energy calculation of the machine. This means that the accuracy of the various inductances calculated from energy perturbation, as well as other machine parameters, will not be affected. The purpose of this approximation is to reduce the number of the elements for the discretization of the housing part,

Values	Quantities
4	Number of poles, NPLOES
36	Number of slots, NSLOTS
0.02	Length of the main gap, AIRGAP (inches)
3.30	Stator lamination inside diameter, DIS (inches)
5.36	Stator lamination outside diameter, DOS (inches)
1.65	Axil length of the stator, STACKL (inches)
0.92	Stacking factor, STAF (per-unit)
0.050	Slot dimension, B0 (inches)
0.151	Slot dimension, B1 (inches)
0.154	Slot dimension, B2 (inches)
0.230	Slot dimension, BS (inches)
0.020	Slot dimension, H0 (inches)
0.010	Slot dimension, HT (inches)
0.050	Slot dimension, HY (inches)
0.483	Slot dimension, HS (inches)
7	Number of slots between coil sides plus one, NYY
0.030	Insulator thickness, TINSU (inches)
1.70	End turn axil length of the armature, ETL (inches)
0.10	End turn dimension, ET1 (inches)
0.25	End turn dimension, ET2 (inches)
4.49	Filed coil inside diameter, DIF (inches)
5.584	Field coil outside diameter, DOF (inches)
1.575	Field coil width in axil dimension, WFIELD (inches)
5.66	Housing inside diameter, DIH (inches)
6.20	Housing outside diameter, DOH (inches)
5.19	Housing inside length, HIL (inches)
5.79	Housing outside length, HOL (inches)
2.19	Endbell inside diameter, DIEB (inches)
2.48	Endbell dimension, DEB1 (inches)
2.95	Endbell dimension, DEB2 (inches)
4.25	Endbell dimension, DEB3 (inches)
1.32	Endbell dimension, HEB1 (inches)
0.325	Endbell dimension, HEB2 (inches)

Table 2.1 Data Base of Stator Design Geometries and Parameters

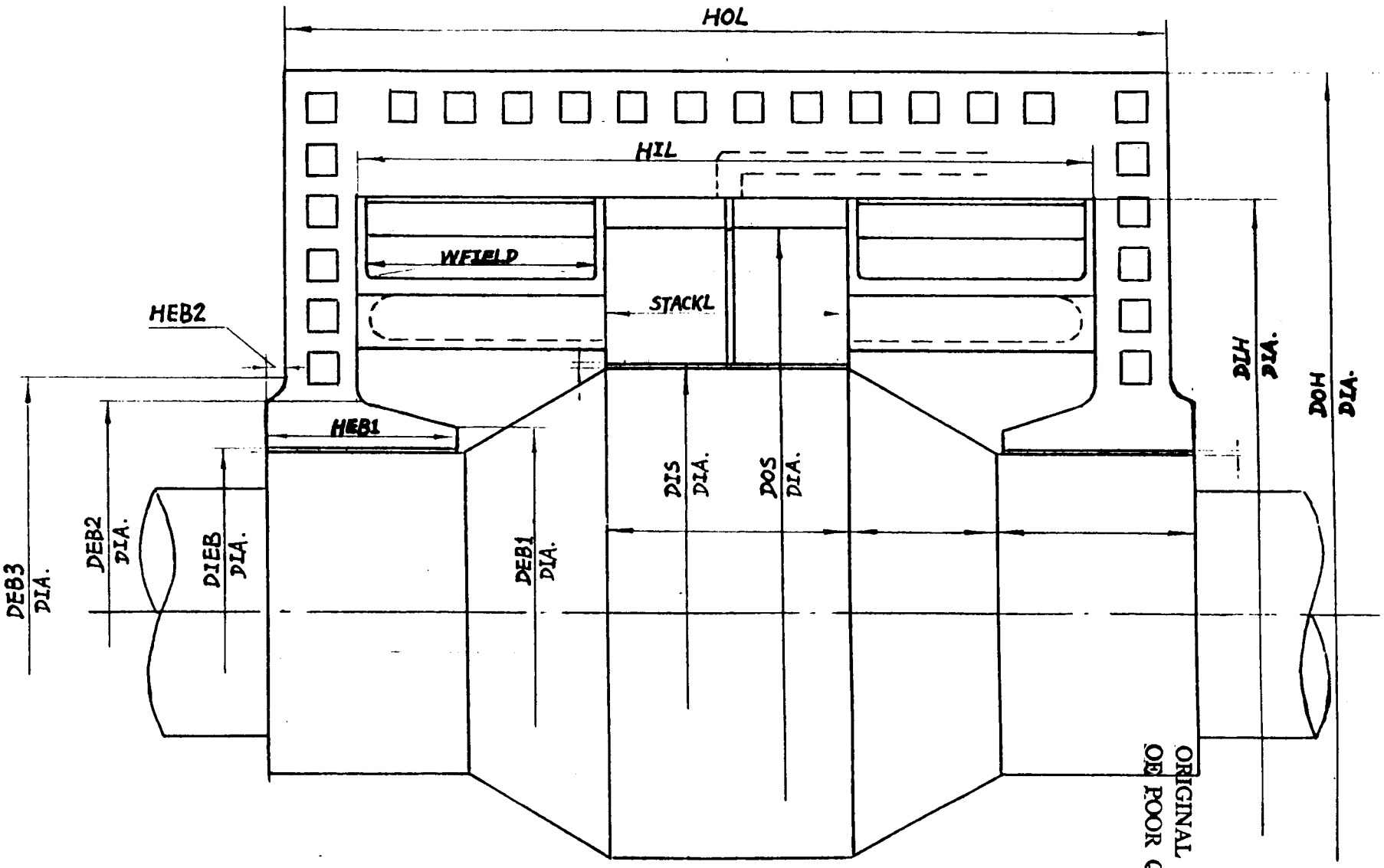

Figure 2.3 Example 14.3 kVA MLA Cross-Section

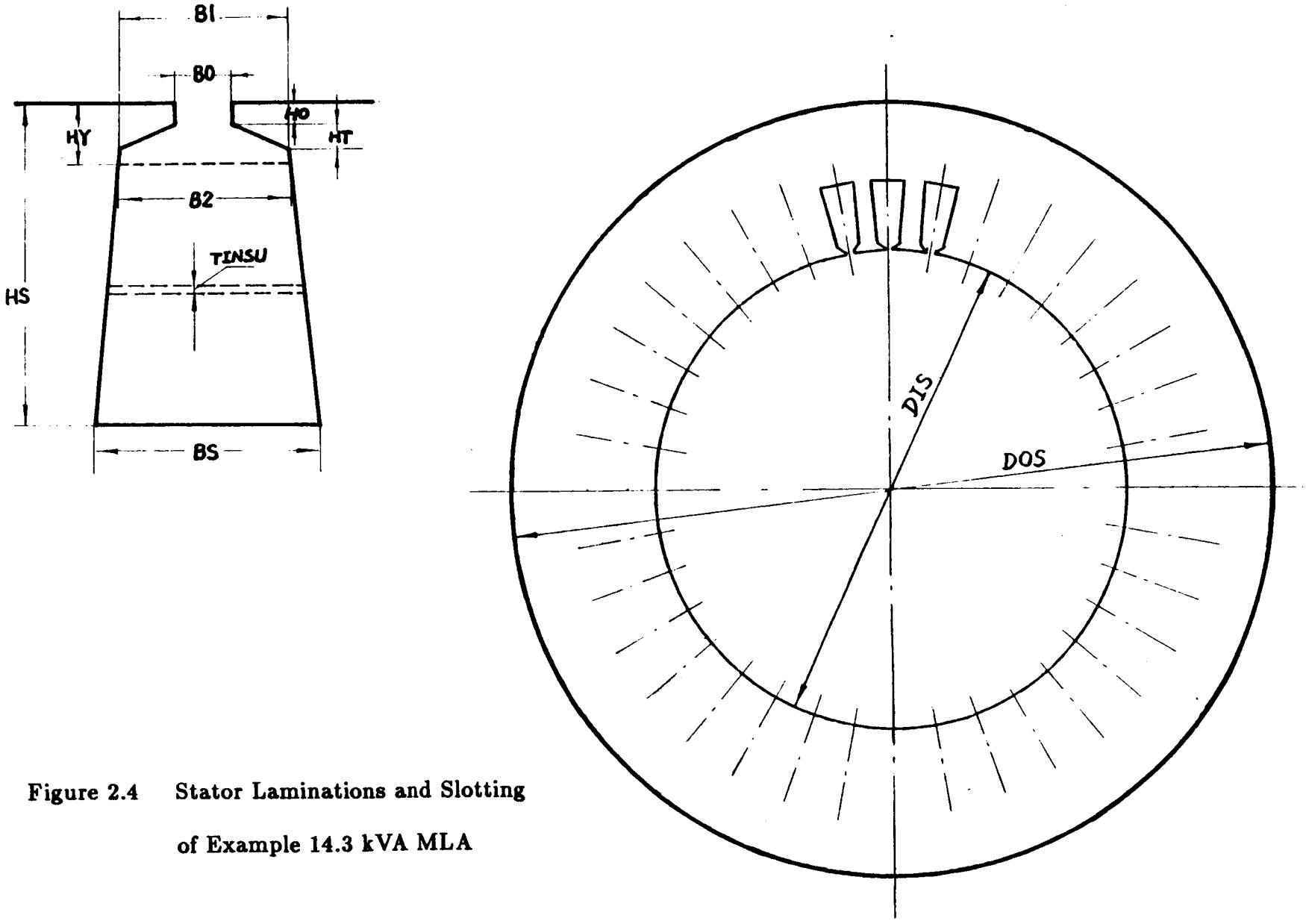

Figure 2.4 Stator Laminations and Slotting of Example 14.3 kVA MLA

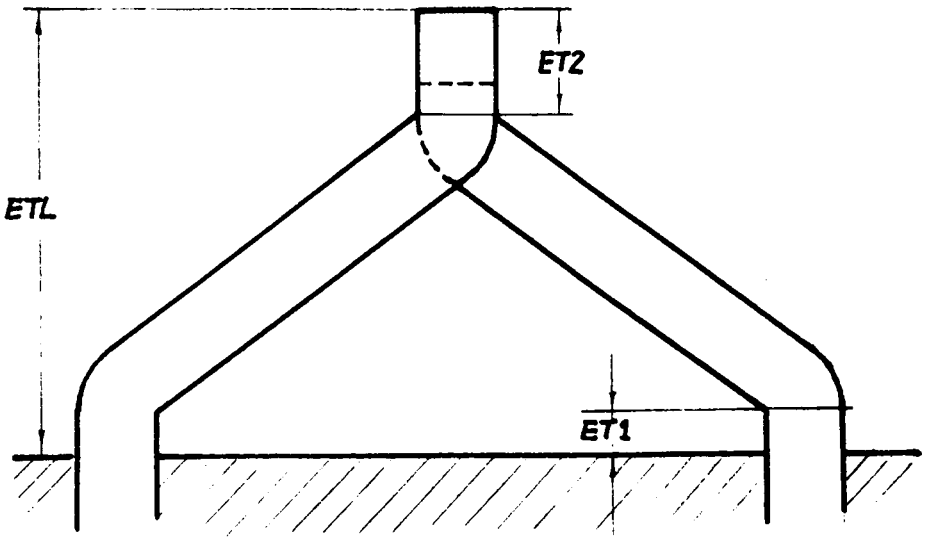

Figure 2.5 Armature End Turn Geometry

where the details of the magnetic field distribution are not critical to the overall performance as was mentioned above. performance as was mentioned above.

The example 14.3 kVA MLA machine decribed above is a four pole alternator with symmetrical three phase armature windings. The structure of the magnetic circuit geometry, the excitation current distribution, as well as the armature current distribution have an identical nature for each pair of poles of the machine. Therefore, the magnetic field disribution in the machine must have the same symmetric property for each pair of poles. This means that the magnetic field calculation may be performed only within the volumetric region of a pair of poles of the machine to save computer time. The restriction of the volume of the solution region to a pair of poles will be used throughout this stage of magnetic field computation in this research project. Accordingly, one half of the machine volume, which occupies 360 electric degrees, which is equivalent to 180 mechanical degrees in the example MLA, with total machine axial length, is chosen as our solution region for the finite element calculation. Thus, the total energy of the magnetic field inside the machine will be twice as that value calculated from the solution region.

3.0 BASIC BUILDING BLOCKS AND NATURE OF THE FINITE ELEMENT GRIDS

3.1 Tetrahedral Finite Element

To carry out three dimensional finite element computation, the machine geometry must be discretized into small three dimensional subregions called finite elements. Each of these elements is identified through a node-element connection designation scheme, which will be refered to as the connection matrix of the given finite element grid. For each element in this three dimensional grid there must be a material identity number, as well as designated excitation current density components, to uniquely represent a particular part of the solution region, with correct geometry, magnetism, and current source characteristics. Again, these finite elements serves as building blocks to form the three dimensional grid. The basic building block or finite element used in this investigation is a first order tetrahedral element, Figure 3.1. This type of element has been used successfully by Demerdash et al. in former works of 3-D finite element magnetic field calculation [3] [4] [5] [6].

It is not convenient to directly handle tetrahedral elements to build up three dimensional grids because of the difficulty in visulization and computer implementation for these elements in forming the finite element grid throughout the solution region. The complex nature of the machine geometry model of the MLA, which contains the end turn region of the armature winding, as well as extremely difficult surface geometries of the interfaces between the magnetic poles and the separator of the rotor, adds substantial difficulties to the discretization work. Two types of techniques have been used to assist in the generation of the finite element grids.

In one of these techniques, one uses triangular prisms as super-elements to build up three dimensional grids for some portions of the machine. Here, the second technique, will be called the filling technique. In this filling technique one divides a space into a number of straps (bars or toroids) with triangular cross-sections, each strap is then filled by tetrahedral elements one by one, for one strap after another, see Figure 3.2 for a schematic demonstration. Such a filling technique was developed in this investigation, and is used here for the first time for the implementation and development of the complex 3-D finite element grid at hand. These two techniques have been used successfully for the discretization of the stator geometry of the MLA machine. Ideas for applying these techniques to deal with the rotor grid generation are presently being developed without difficulty. Detailed work on the stator grid and the rotor grid will be reported in Section 4.0, and Section 5.0.

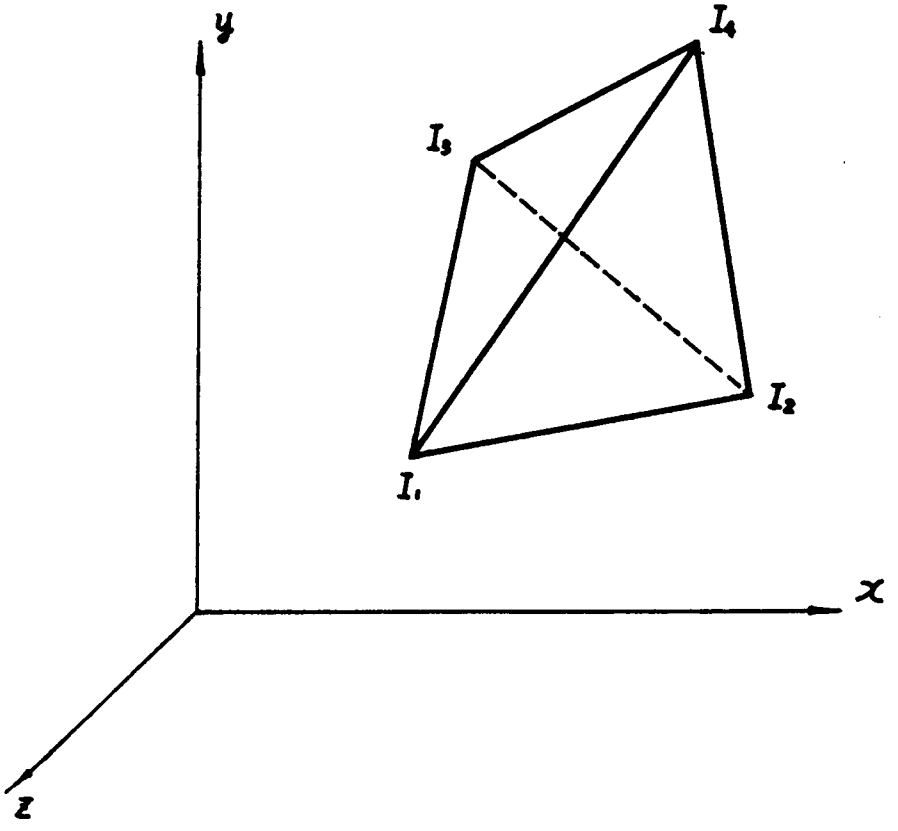

Figure 3.1 Tetrahedral 3-D Finite Element

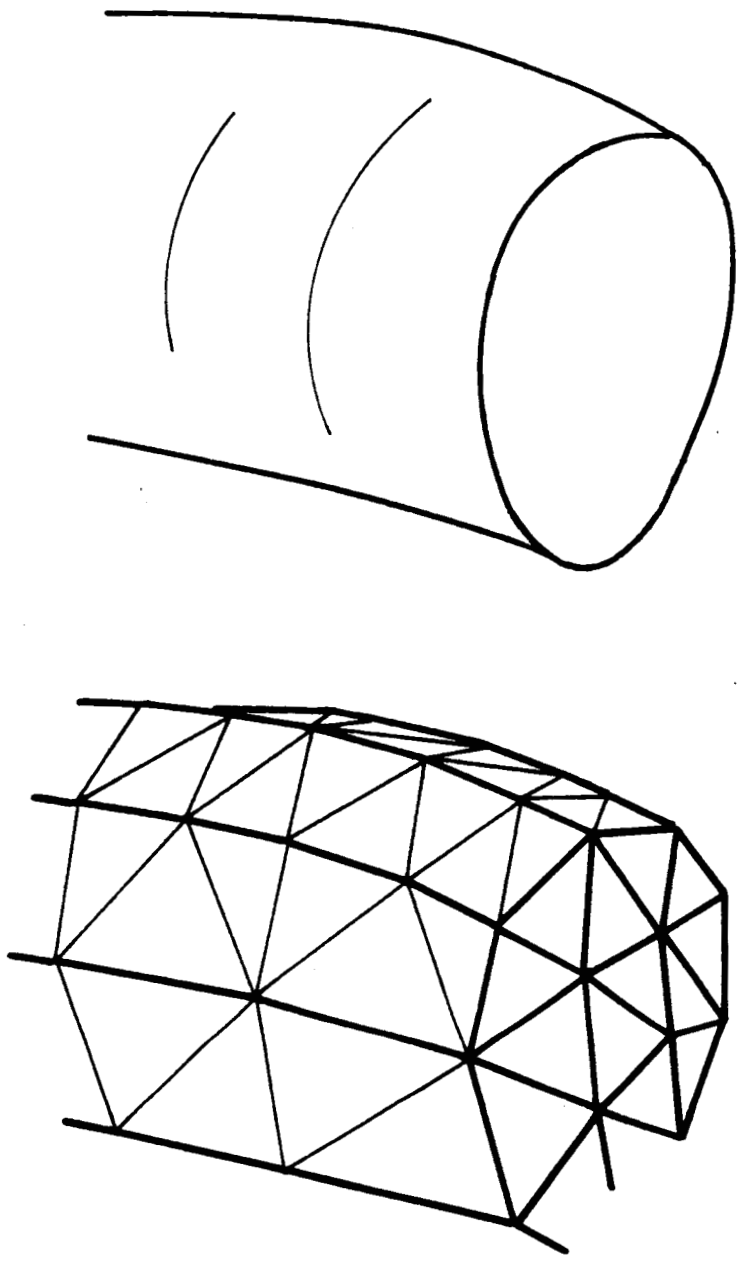

Figure 3.2 FE Grid Filling Technique

3.2 Triangular Prism Super-Elements

As an aid in constructing the various portions of the finite element grid for some parts of the machine geometry, triangular prisms are developd as super-elements to help discretize the three dimensional space for the first step in the process of generation of the global three dimensional tetrahedral finite element grid. Each of these triangular prisms is then divided into three tetrahedrons to complete the grid topology. There are two basic ways to divide a triangular prism into three tetrahedrons, as shown in Figure 3.3. Alternately using these two types of super-elements makes it possible to avoid crossing of edges of tetrahedrons from two super-elements, which might happen at the interfaces, and which must not take place in a 3-D finite element grid. A triangular prism can be itself a finite element. However, because of the restrictions on geometric shapes which are ammenable to discretization by prism shapes, these investigators restricted the use of prisms to the task (technique) of assisting in the generation of the grid in tetrahedral elements form. The final grid model of the machine, which is described by a generated data structure set, is based on tetrahedrons as the basic building blocks.

Using a triangular prism or even considering two triangular prisms forming one hexahedral block as a super-element, is a very efficient and convenient way to construct the necessary three dimensional grids. Many machine parts such as the field coil, the housing, and the rotor shaft, can be cut into pieces with a number of planes or surfaces carrying identical surface triangular grids. Then three dimensional triangular prisms can be filled into the space separating the two surfaces by simply taking one triangle from each of the concerned surfaces to form a triangular prism in which the top base and the bottom base are the aforementioned two triangles, and the process is repeated throughout the space between the two

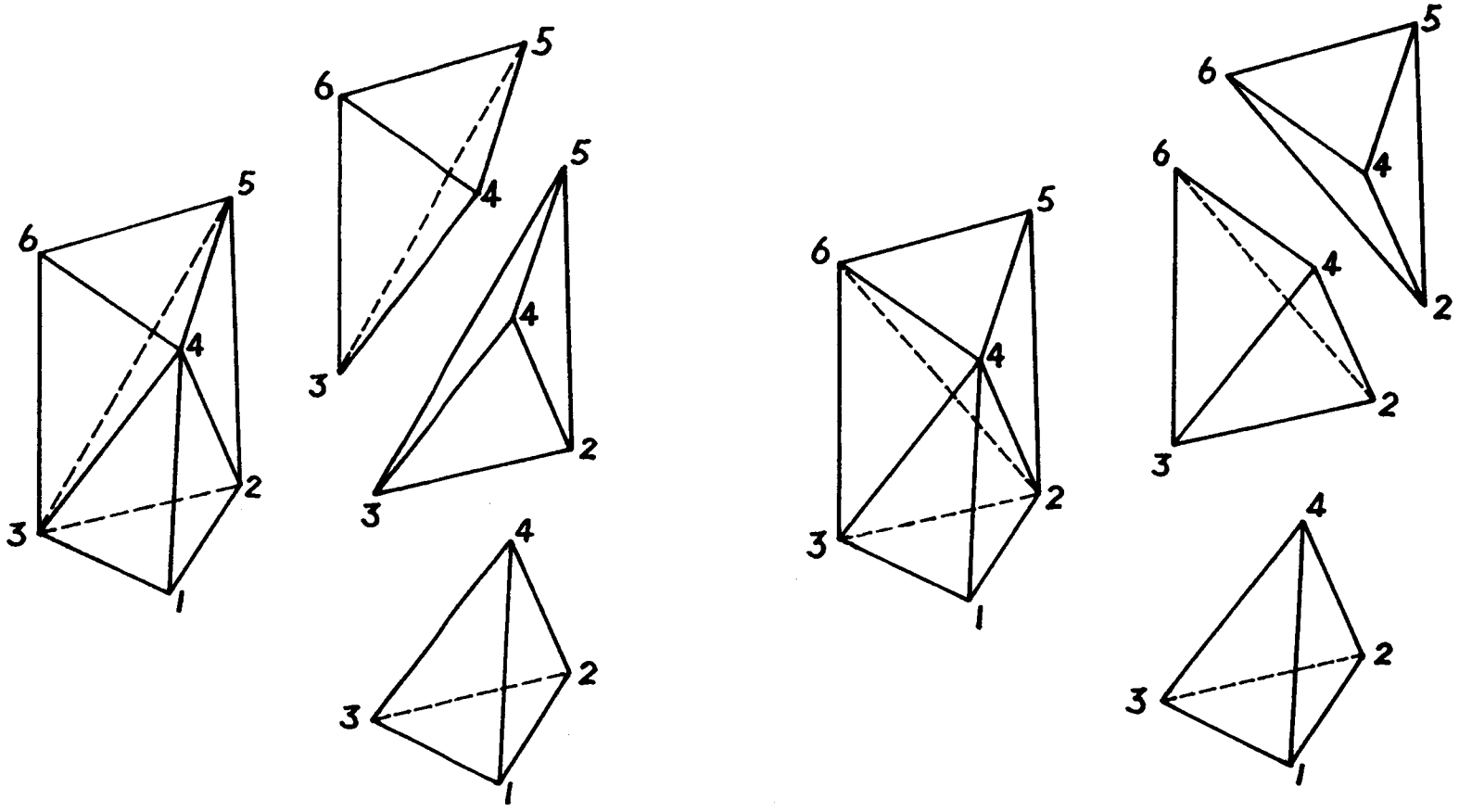

Figure 3.3 Triangular Prism Super-Element Break Down to Tetrahedrons

surfaces. However,there are some circumstances in which the triangular prism super-elements are not suitable. For example, when elements must be filled into a gap between two machine parts, where the two surfaces of the gap have arbitrary surface triangular patterns, the above method will not work. Thus a filling technique must be developed to tackle these difficulties. This is described next.

3.3 Filling Technique

As mentioned previously, a filling technique has been developed to generate the tetrahedral fineite element grids where triangular prisms can not be used effectively. The main idea of this technique is that one can fill tetrahedrons one after another into a triangular strap (a bar or toroid with triangular cross-section) when two side walls (or surfaces) of this strap have been already discretized into arbitrary triangular grids. After one strap is fully filled with tetrahedrons, the third side wall of the strap automatically becomes discretized into a certain pattern of a triangular surface grid, which will be in turn used to determine the tetrahedral finite element filling manner of the adjacent strap. Such a filling process will be further explaind by an example later in this section.

Actually, it is not necessary to use this filling technique thoughout the whole machine geometry, because many parts of the machine can be discretized easily by triangular prism super-elements from which tetrahedral finite elements are generated. The whole grid structure can be completed by first building several small grid modules separately with super-elements then connecting the modules together by the above mentioned filling technique. This filling technique has been found very usefull in matching the stator grid and the rotor grid to complete a global tetra-

hedral finite element grid for the class of alternators at hand. Such a matching is important because the magnetic field calculation will have to be performed at different rotor positions, to include the effects of rotor geometry and stator slotting on machine parameters and other performance characteristics.

The following is an example of the application of the above mentioned filling technique. Consider the geometry given in Figure 3.4, a gap between two surfaces, with fixed surface triangular grids on each, is to be filled with tetrahedral elements. In order to apply the filling process, the space of the gap is separated into five straps as shown in the lower part of Figure 3.4. Each of the straps has one of its three side walls (surfaces) with a given set of surface triangles. These straps (bars) will then have to be filled with tetrahedral elements one strap after another, by repeatedly calling a computer subroutine. Since this subroutine is developed in a manner suited for general use, it requires that the strap undergoing the tetrahedral filling process must have two side walls already with given surface triangular grids.

Thus, before the subroutine is called, one side wall, S_1, of the first strap, which must not be the interface with the second strap, as shown in Figure 3.4, has to be discretized into a suitable set of triangles. At the end of the execution of the subroutine processing the first strap, a surface triangular grid will have been established on the third wall (surface), S_3, of the strap (bar), which is the interface between the first strap (bar), 1, and the second strap (bar), 2, see the Figure 3.4. At that stage, the second strap is ready with surface triangular grids on two of its three side walls. The second strap is then put through the same process by calling the same subroutine as is explained above for the first one. The third, the fourth, and the fifth straps (bars), see Figure 3.4, will have been filled with tetrahedral elements by sequential application of the above procedure in a chain manner.

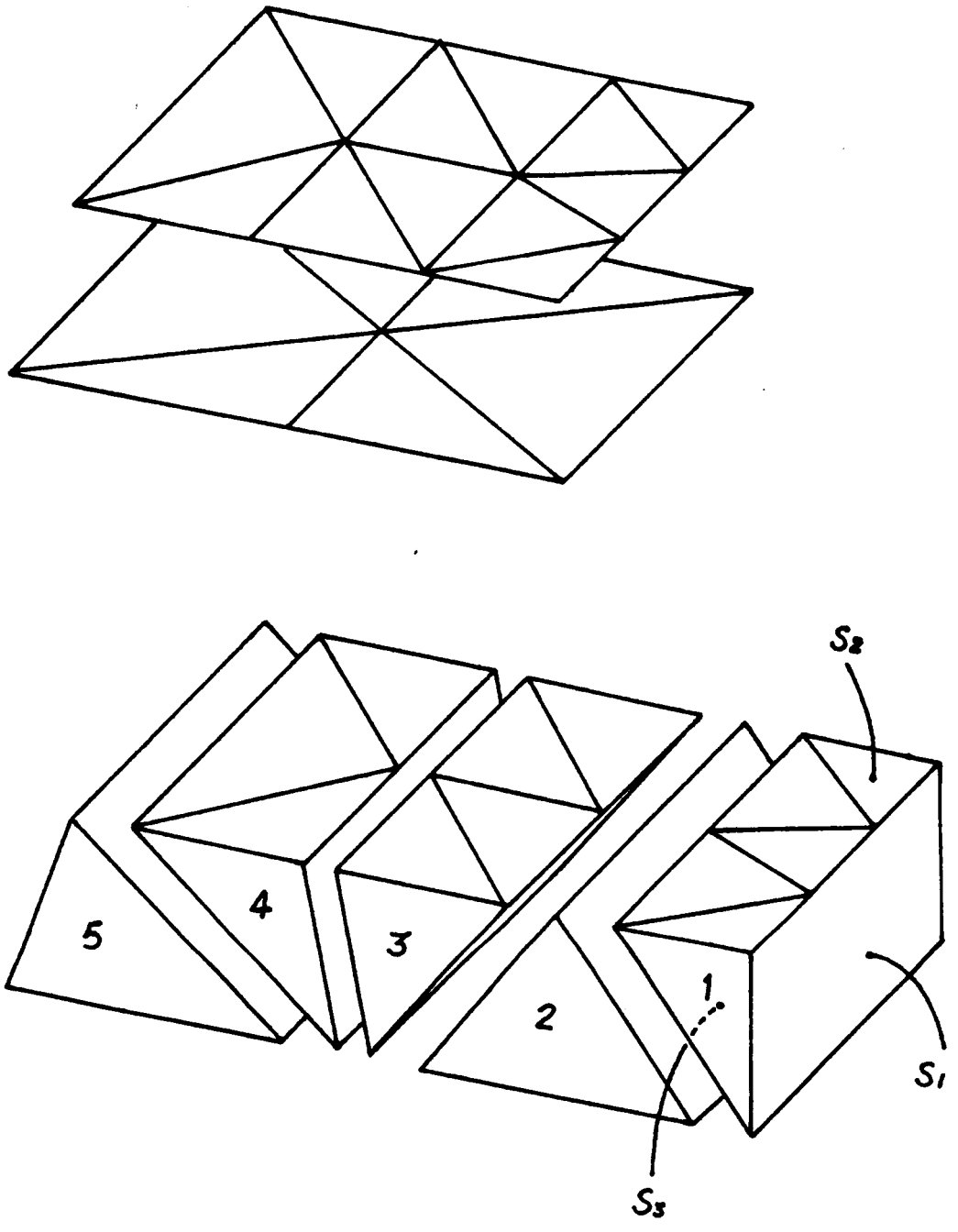

Figure 3.4 Example Filling Technique Between Surfaces

The resulting grid which fills the gap of Figure 3.4 with tetrahedral elements is shown in Figure 3.5.

Next, consider the first strap (bar) in Figure 3.4 as an example to demenstrate how a tetrahedral grid is computer generated to fill the bar volume under consideration. Let one imagine that this strap is now put in an upright position as shown in Figure 3.6, graphs (1) through (3), for the convenience of visualization. The front side wall (surface) with nodes 1, 7, 8, 9, and 2 is the wall without a given triangular grid. Each tetrahedron will be generated by a sequential procedure which can be generally summarized as follows:

1. Chose a triangular base for the tetrahedron,
2. Find a new node as the fourth vertex of the tetrahedron,
3. Link the new node to each vertex on the base to complete a tetrahedron.

Applying the three steps given above, the triangle with nodes, 1, 7, and 3, designated by (1,7,3,1), Figure 3.6, graph (3), is chosen as the base for the first tetrahedron. A searching process is then carried out, which shows that triangle (1,3,4,1) and triangle (3,7,4,3), Figure 3.6, graph (3), share edges, 1-3, and 3-7, with the triangular base (1,7,3,1), respectively. Thus, from this information, only node, 4, is eligible to be the new vertex of the tetrahedron being formed. Accordingly, nodes 1, 7, 3, and 4, make the first tetrahedral element {1,7,3,4}, as shown in Figure 3.6, graph (4). Node, 4, then takes place of node, 3, to make a new triangular base (1,7,4,1) for the second tetrahedron under formation.

Repeating the same searching process as explained above for the first tetrahedron, triangle (1,4,2,1) and triangle (4,7,8,4) are found to share edges, 1-4, and

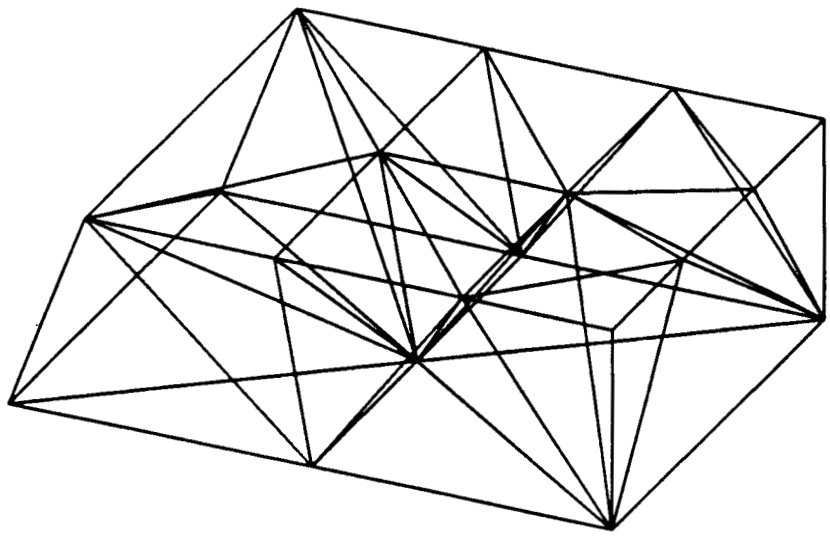

Figure 3.5 Example Generated FE Grid for Example in Figure 3.4

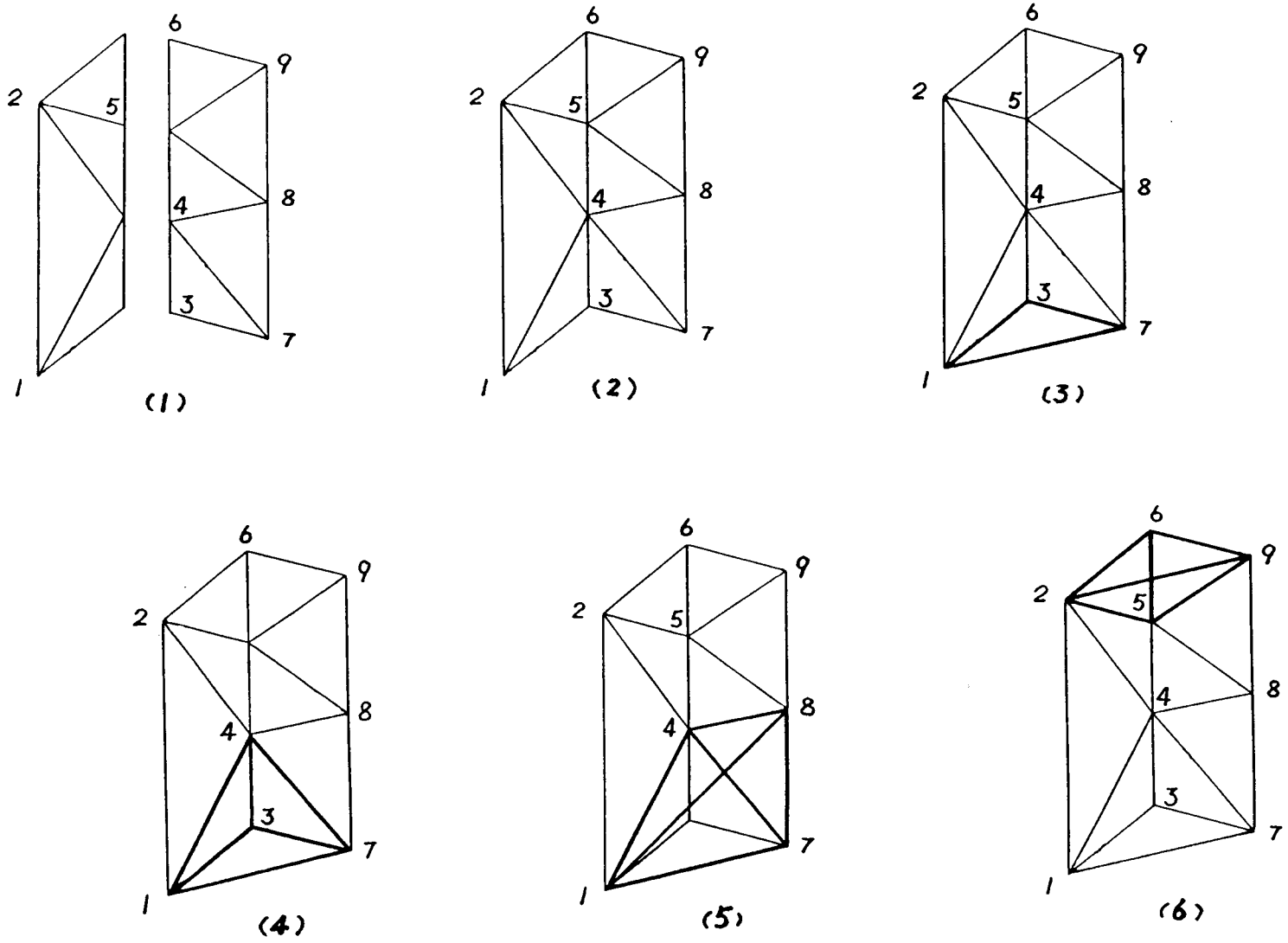

Figure 3.6 Triangular Bar Discretization into Tetrahedrons

4-7, with the base triangle (1,7,4,1) being currently considered, respectively. Under this condition, either node, 2, or node, 8, can be considered as the candidate for the new vertex of the second tetrahedral element. A criterion has to be developed to decide as to which node should be chosen to yield a resulting tetrahedral element with the least possible 3-D geometry illconditioning. This criterion established here can best be adhered to using the following concept: chose one node among these two candidate nodes such that the edge appearing on the front wall, 1-7-8-9-2-1, will be the shortest. Thus node, 8, is chosen as the new vertex, because the distance from node, 1, to node, 8, is shorter than the distance from node, 7, to node, 2. After linking node, 8, to the three vertices on the triangular base, (1,7,4,1), an edge eminating form node, 8, to node, 1, as well as a triangle with nodes, 1, 7, and 8, appear on the front wall of the strap, Figure 3.6, graph (5). Now, the triangle (1,8,4,1) can be chosen as the new base for the third tetrahedron to continue the tetrahedral element filling process. In this process one repeats the above mentioned procedure as many times untill the last tetrahedron {2,9,5,6} with nodes, 2, 9, 5, and 6, at the top of the strap is completed, Figure 3.6, graph (6). Figure 3.7 is a view of the finished tetrahedral grid filling the strap.

It should be mentioned here that the aformentioned search process to find candidates for the new vertex of each new tetrahedron has to be carefully formulated in such a manner that no edges of any tetrahedrons generated in the grid ever intersect. Application of the concept of grid generation using triangular prism super-elements, and the filling technique discussed earlier in this section, for purposes of stator and rotor grid generation is discussed in following section of this report.

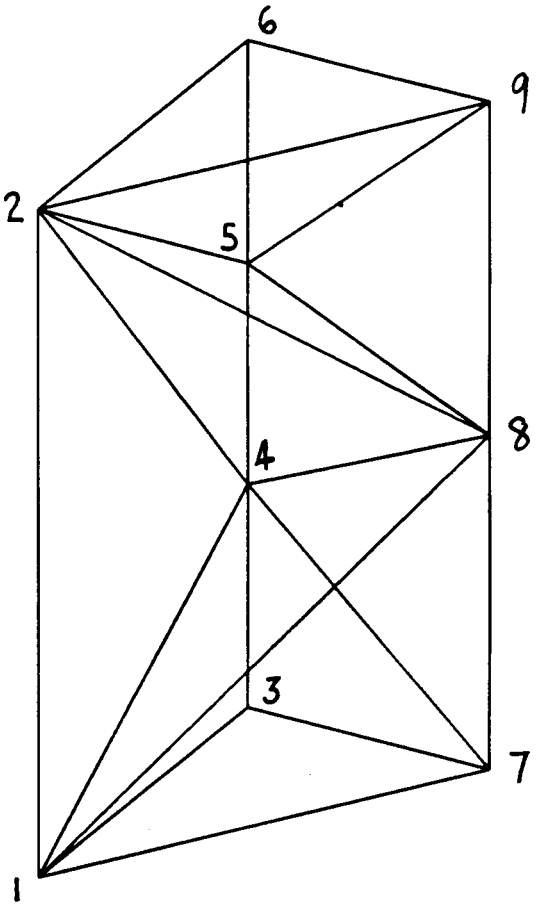

Figure 3.7 Final Triangular Bar FE Tetrahedral Discretization

4.0 STATOR FINITE ELEMENT GRID GEOMETRY

According to the flow chart discussed earlier in Section 1.0, which shows the sequential order of algorithms to be developed in the course of this investigation, the stator finite element grid is to be generated first, followed by a rotor grid to which it is to be "stitched" to form the desired global grid system. The selection of the various rotor positions is dictated by the nature of the performance characteristics being investigated, as will be explained later in this and future reports.

A cylindrcal surface, which has the same diameter as that in the middle of the main airgap, and axially extends to both ends of the machine magnetic circuit, is considered to divide the machine geometry into two parts. The outer part is a cylindrical shell which contains the armature, half the cylintrical shell constituting the main airgap, the outer frame and a portion of the endbell, and it occupies the volumetric region belonging to the stator. This volumetric region is called the stator grid. Meanwhile, the inner part is an inner cylindrical shell which contains the rotor, the remaining half of the cylindrical shell of the main airgap, and the remaining portion of the endbell, and it occupies the volumetric region belonging to the rotor. This volumetric region is called the rotor grid.

The stator grid and the rotor grid are then generated separately to occupy these two aforementioned volumetric regions. The inner surface discretization of the stator grid, as viewed from the rotor side, will have been formed in this investigation in such a way that the stator grid and the rotor grid can be connected easily at each of the various rotor positions under consideration.

A computer program using standard Fortran-77 language has been developed

successfully to generate the stator finite element grid. The features of the stator finite element grid, the generated grid pictures, as well as some programming considerations are reported in this section.

4.1 Basic Grid Module for the Stator Grid

An overview of the configuration of the MLA machine shows that the geometry of the stator part has symmetric properties as follows; the geometry construction in each slot pitch of the machine is identical, and the stator has a mirror symmetry structure with respect to a radial cross-sectional plane at the mid point of the machine (perpendicular to its axis of rotation). These properties allow one to build the stator grid by assembling small grid modules with identical finite element grid topology. Such a consideration of using a small grid module has greatly reduced the work for the generation of the stator finite element grid.

Figure 4.1 shows an isometric view for our basic building block, or grid module, for the stator finite element grid. This module occupies a space volume within one slot pitch and half an axial length of the machine, that is, it occupies a region starting at the outer boundary of the endbell and ending in the middle of the stator laminations (stack). The front surface which contains cross-sections of the end turns and field windings as shown in Figure 4.1, and the back surface which is hidden in this figure, have the same surface discretization, that is the same triangular pattern. Thus, as many numbers of these modules as deemed necessary can be put together, side by side in the circumferential direction to accumulate the stator grid, without any grid geometry conflict at the interface between adjancent modules. The grid is then mirror imaged into another half length of the machine

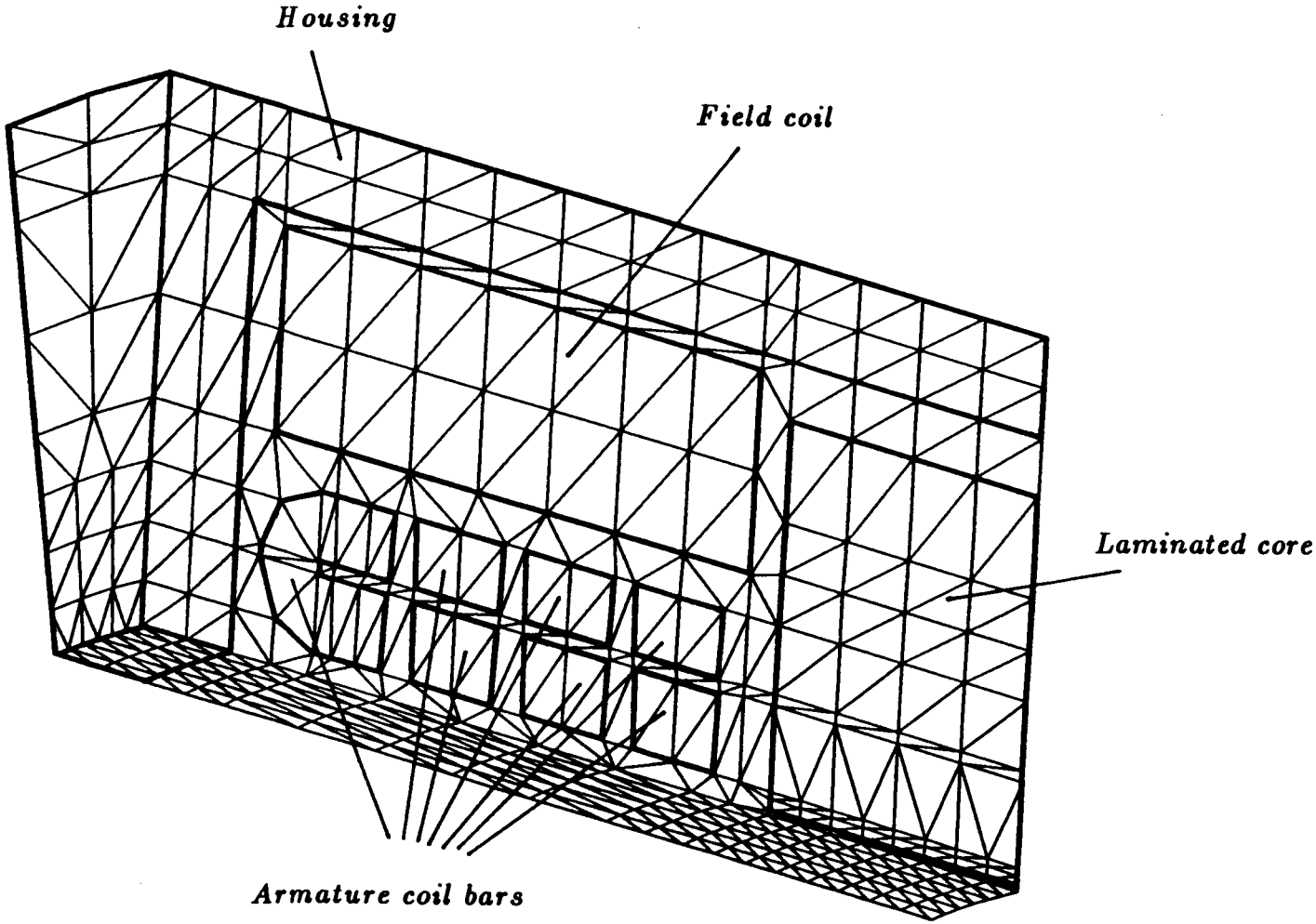

Figure 4.1 Basic Module of Stator Finite Element Grid

to complete the whole stator finite element grid model.

As identified in Figure 4.1, such a grid module has included all machine parts, insulators, and free spaces in the occupied volumetric region. In this finite element grid module, each tetrahedral element has a material identity number, and elements of the same machine part have the same material identity number. Thus, after the overall stator grid is completed, each machine part can be presented by picking up all of its tetrahedral elements from the grid, based upon the material number uniquely assigned to that machine part.

The field winding and the armature winding may carry currents. The relative magnitude and the direction of the current density vector distributions in each concerned element have to be generated for utilization in further finite element computations. This process is to be repeated for the various machine load conditions. More detailed work about the generation of the tetrahedral grid for this stator grid module of Figure 4.1 will be shown soon in Section 4.3.

An outer surface view of the generated stator finite element grid is presented in Figure 4.2. Notice that no internal grid lines are shown in this figure, and that all the triangles shown represent faces of tetrahedrons in the finite element grid whose side surfaces lie along these outer surface boundaries of the stator grid. This finite element grid model covers the geometric space of two pole pitches of the machine, which is chosen as the solution region for the magnetic field computation, as mentioned previously in Sestion 2.0.

Notice that the surface discretization on the inner cylindrical surface of the stator grid, as shown in Figure 4.2, can be considered as a combination of small rectangles, with each rectangle subdivided into two triangles. It should be pointed

Figure 4.2 Outer Surface View of Discretized Tetrahedral FE Grid of Stator

out that the partition for these rectangles in the circumferential direction is uniform. Thus, a rotor grid, which will be generated with the same surface dicretization on its outer cylinder, can be connected to the stator grid by sharing the nodes and triangles on the interface. Therefore, such connections can be made at different rotor positions by rotating the rotor grid over one or any whole number of partition distances.

4.2 Stator Grid Presentation

In this section, a number of isometric pictures will be shown to further clarify the nature of the developed stator finite element grid. The basic computer graphics tool used to plot these grids is the *IGL* library of subroutines, a commonly used graphics software package available recentely in most main frame computer systems. Frotran programs were developed to employ the basic graphics subroutines from *IGL* to plot these 3-D tetrahedral element grids. These computer plotting routines have capabilities as follows:

1. Plotting of overall 3-D tetrahedral grid with inside lines.
2. Plotting of portions of the grid with a common element material identity number, with inside lines.
3. Plotting of surface triangular grids, where each surface is a plane parallel to the XOY, YOZ, or the XOZ coordinate reference plane, It can also plot a cylindrical surface with its axis of symmetry coinciding with the Z-axis.
4. Plotting of surface triangular grids, where the surfaces are the interfaces between regions with different materials.

The plotting methods listed above can basically meet the requirements of graphical display and presentation of the 3-D grid geometries at hand, as will be shown in the following pages of this report. However, sophisticated graphics software and hardware, for example, deleting hidden lines, and color pictures, are needed to obtain high quality 3-D grid pictures. The following are the isometric pictures which can best represent the generated tetrahedral finite element grid for the stator geometry at the present status of this investigation:

a) Figure 4.3 shows the grid portion covering the laminated armature core. All inside lines and the triangles on stator slot walls were eliminated.

b) Figure 4.4 is the portion of the grid covering the armature core over a region of one slot pitch. It is a portion of the aforementioned basic stator building block module in Figure 4.1.

c) Figure 4.5 represents the portion of the stator grid which covers the field windings of the machine. The inner grid lines were eliminated in this plot.

d) Figure 4.6 shows groups of small arrows representing the excitation current density vectors in the field windings. Each arrow starts from the center of a tetrahedral element, pointing in the direction of the current density vector at the center (centroid) of that element, with a length for each arrow which is proportional to the magnitude of the current density at that centroid.

e) Figure 4.7 shows the finite element grid for the portion of the volume covering an armature coil. Such a grid geometry duplicates the physical geometry of the armature coil of the machine in the three dimensional space. As can be seen from this picture, it includes the straight line part which is actually embeded in

Figure 4.3 Outer Surfaces of Stator Core Tetrahedral FE Discretization

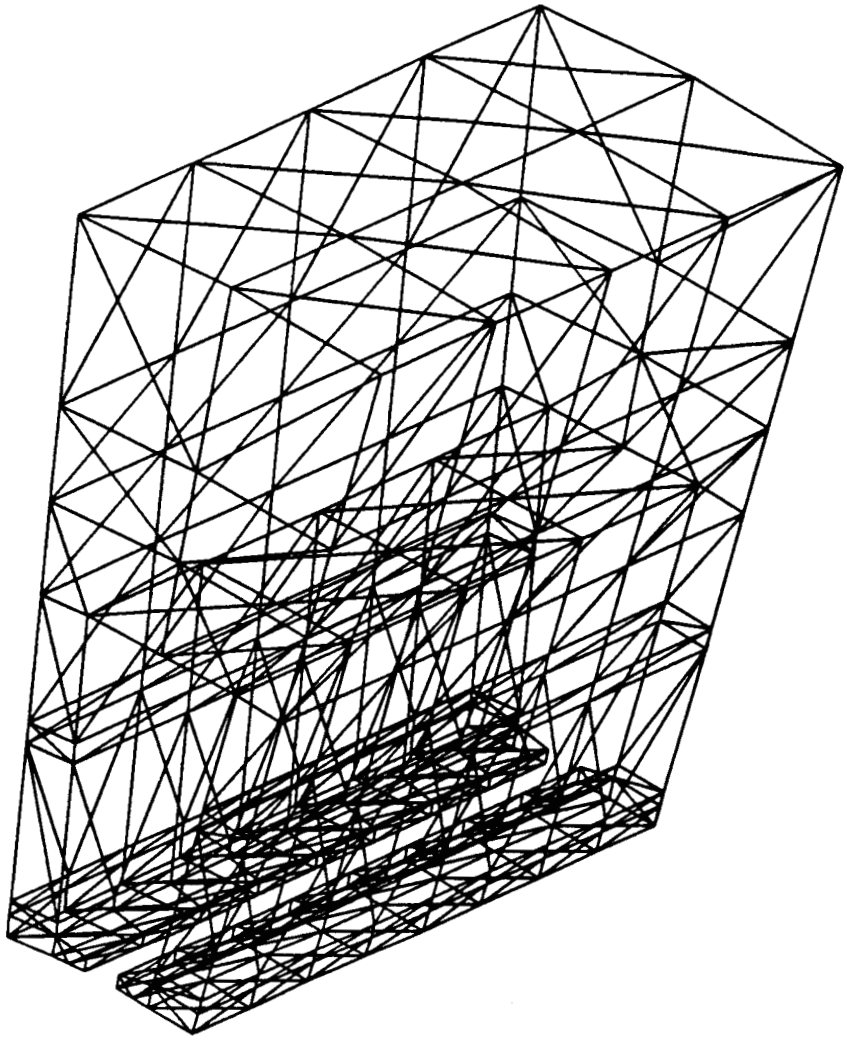

Figure 4.4 Tetrahedral FE Grid of Slot Pitch in the Laminated Core

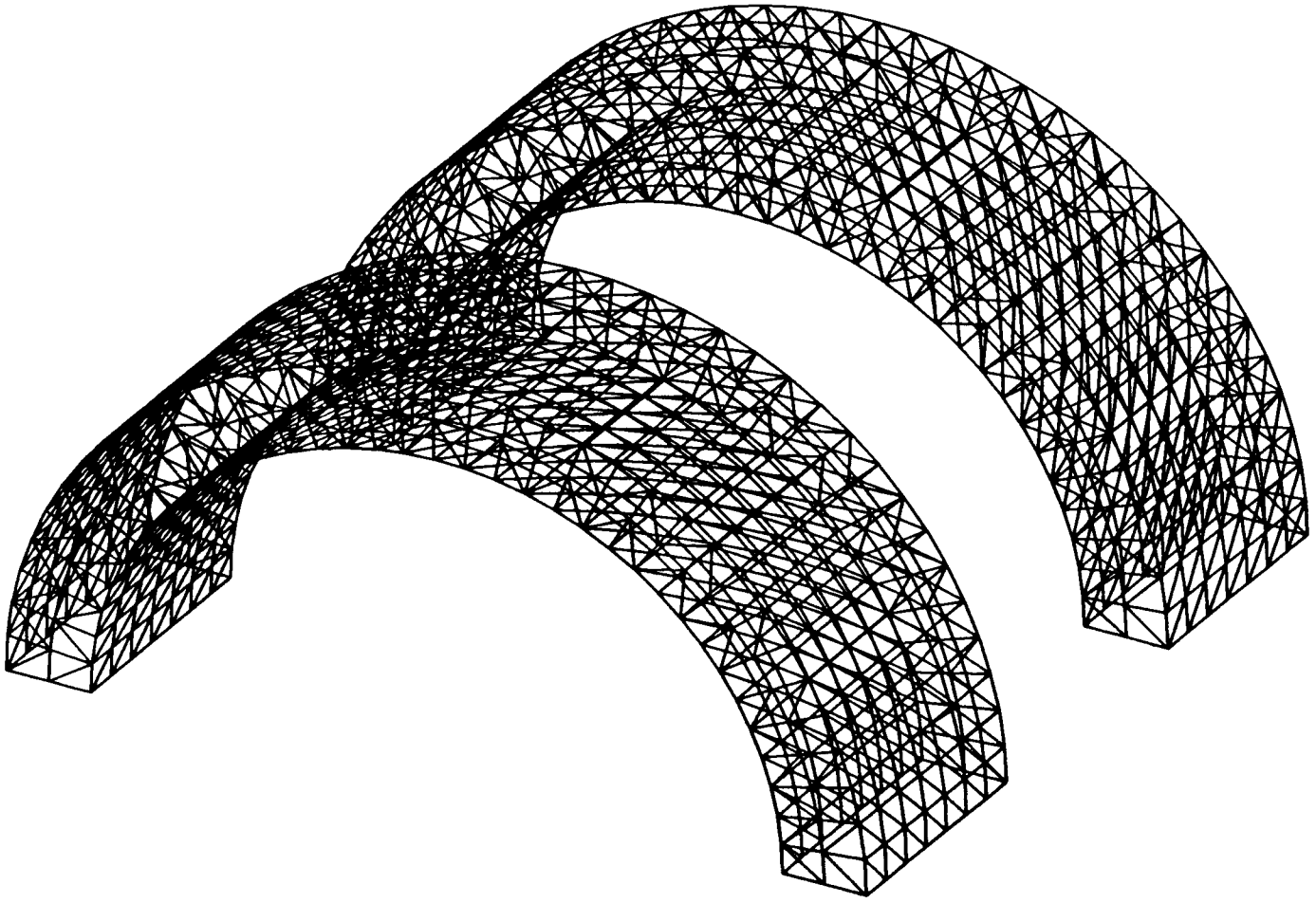

Figure 4.5 Outer Surface Tetrahedral FE Discretization of Field Coils

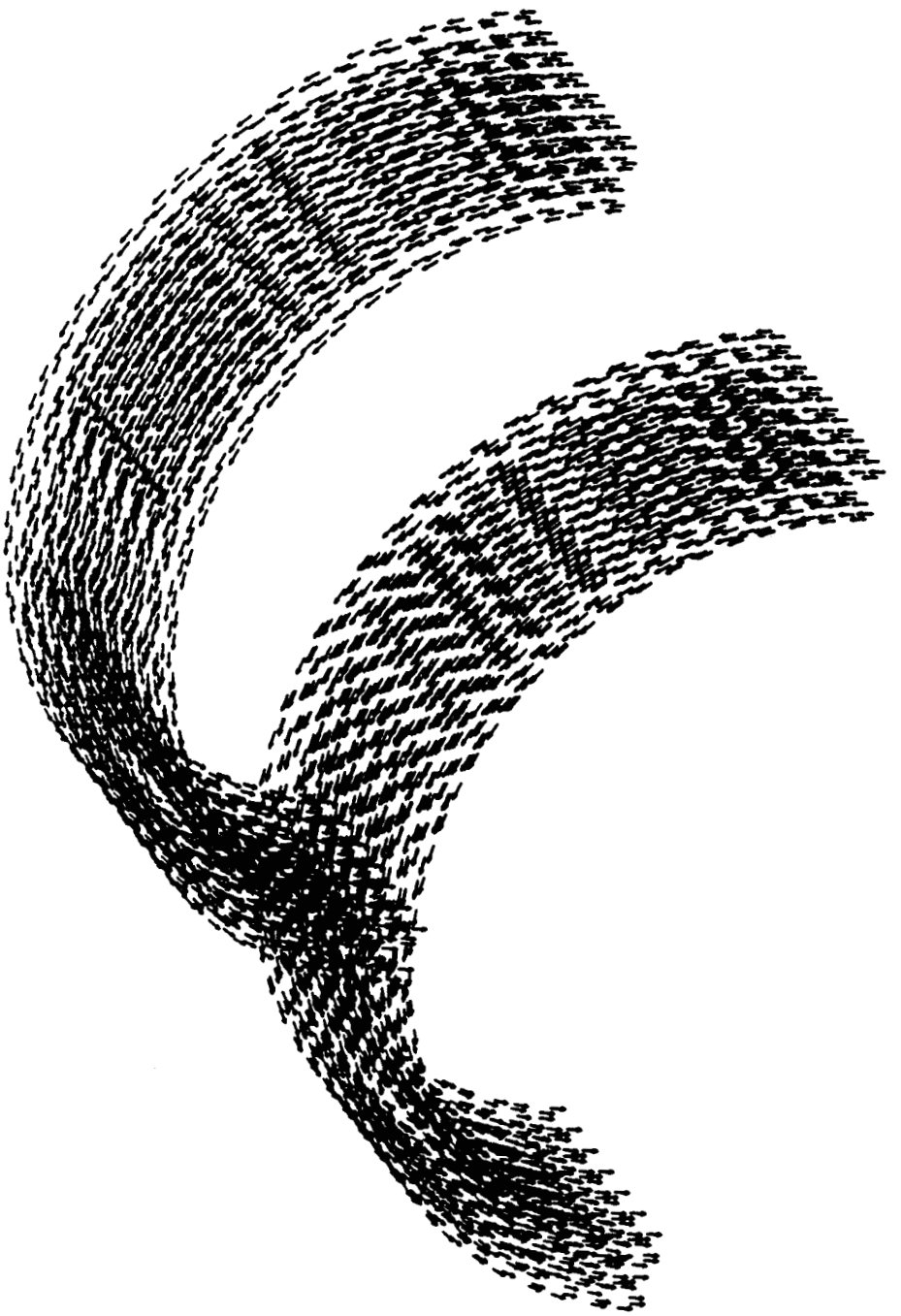

Figure 4.6 Current Orientation in Field Coils

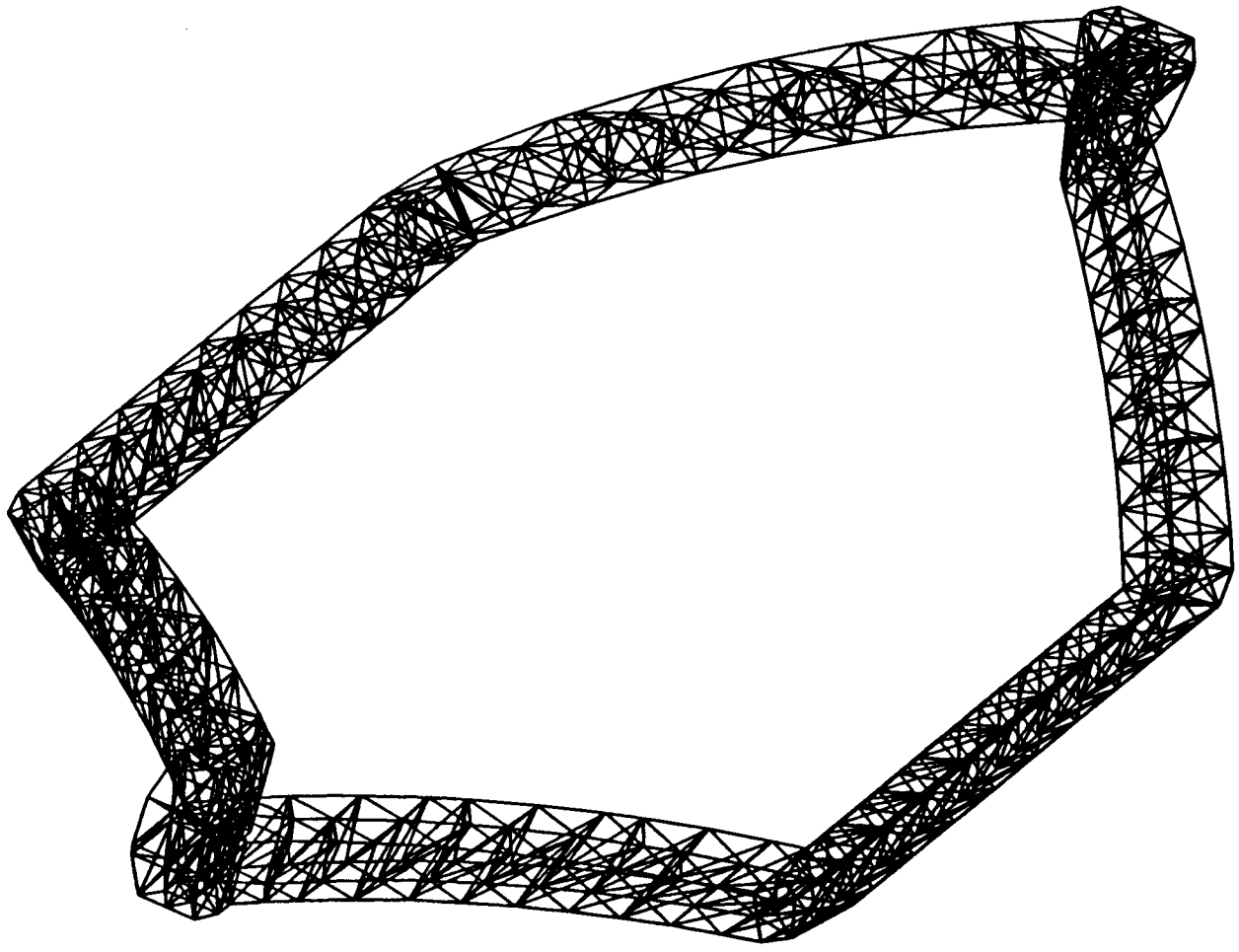

Figure 4.7 Tetrahedral FE Discretization of an Armature Coile

the armature laminations (slots), as well as the end turn part of the coil which forms the coil side connection from one slot to its corresponding return coil side to form a complete coil. Upon closer examination of Figure 4.7, one can recogonize that the right portion and the left portion of the coil shown in the figure are in different layers of the armature winding. That is, one side is in the upper layer and the other side is in the lower layer of the armature winding.

f) Figure 4.8 indicates the current density vector distributions inside an armature coil. Again, these arrows represent both the directions and the relative magnitudes of the current density distribution, as explained earlier for the case of the field winding in Figure 4.6.

g) Figure 4.9 displays a picture which shows how two armature coils overlap in the end turn region of the armature.

h) Figure 4.10 presents the portion of the grid covering the laminated armature core as well as some armature coils with their straight line portions embeded in the stator slots. All inside lines of the grid for laminated core were eliminated. However, the inner lines in the coils were not eliminated to highlight the differences between the core and coil regions.

i) Figure 4.11 is another view for the same grid as shown above in Figure 4.10. and

j) Figure 4.12 shows the portion of the stator grid covering the housing part in the stator magnetic circuit. Only a half portion of the housing is presented here. In the actual model the finite element grid not only contains the portion shown in Figure 4.12, but also contains its mirror image.

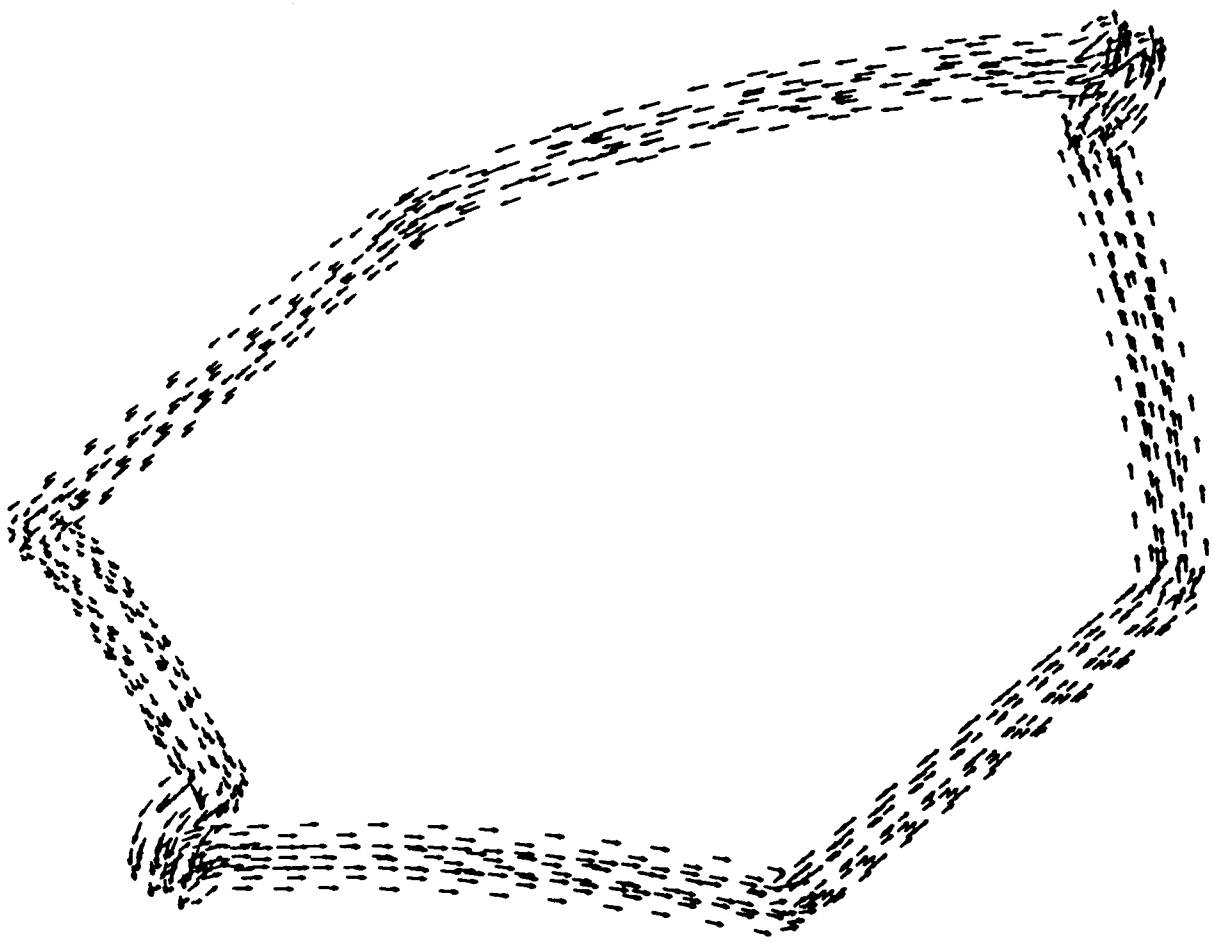

Figure 4.8 Current Orientation in an Armature Coil

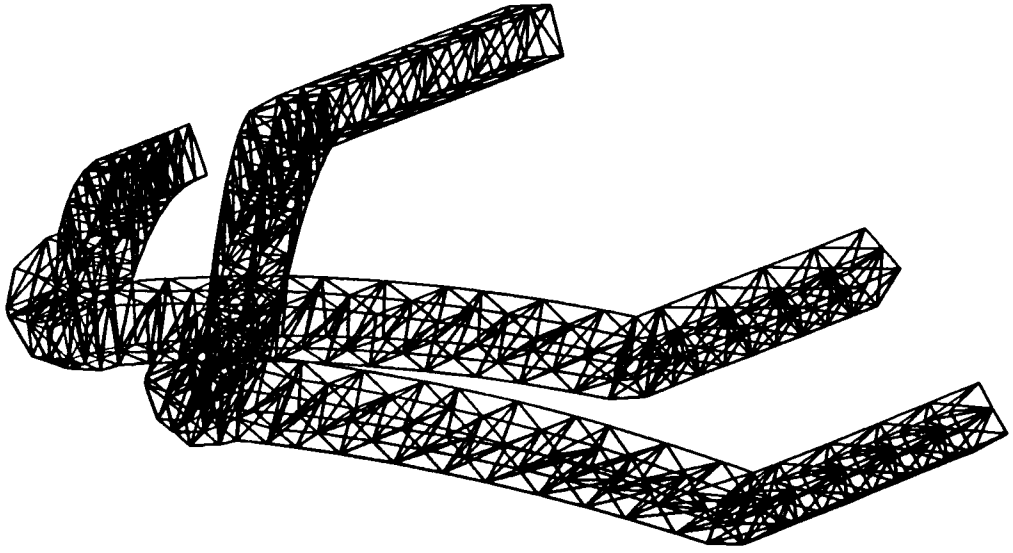

Figure 4.9 End Region of FE Discretization of Two Armature Coils

Figure 4.10 Two Armature Coils Embeded in Stator Core - Case (1)

Figure 4.11 Two Armature Coils Embeded in Stator Core - Case (2)

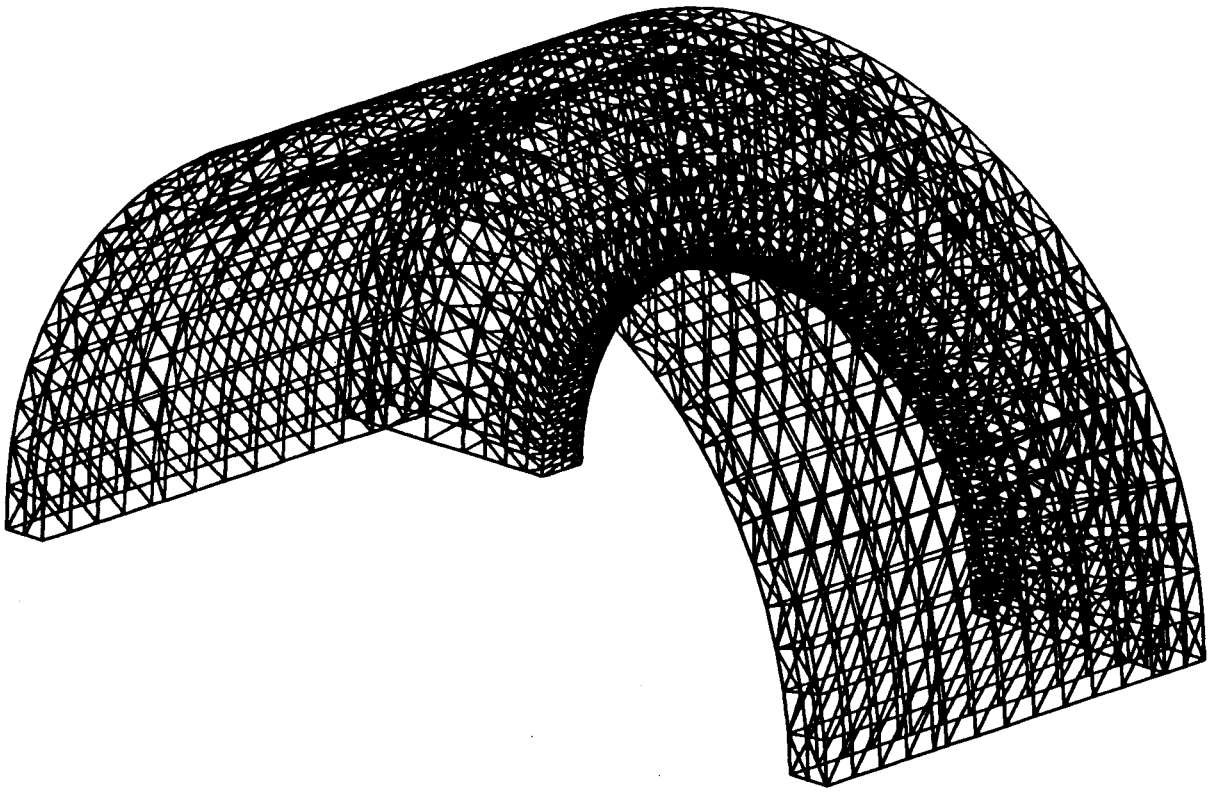

Figure 4.12 Surface View of Tetrahedral FE Discretization of Half the Outer Housing

4.3 Programming Considerations

Some considerations in the development for the basic concepts used in the generation of the stator finite element grid are presented and discussed in this section. As mentioned previously, the major part of the discretization work is dedicated to the construction of the small grid module shown in Figure 4.1. The overall stator grid geometry is filled with tetrahedral elements by repeating the above mentioned grid module as many times as there are slot pitches in a two pole span (two-pole pitches) in this machine.

Figure 4.13 displays a flow chart that shows the main steps in the computer program for the generation of the stator finite element grid. The input data file for the first step of the flow chart is a set of geometry description data for the stator part of the MLA, which has been shown earlier in Section 2.0 of this report. Again, this data file may have to be modified further according to NASA's needs as this investigation evolves. Finite elment grids for different designs of MLA machines can be obtained by simply changing the numbers in the input data file shown here. Such an arrangement is very convenient for allowing engineers, who may not be familiar with finite element computation, to use this computer aided model.

Description of the second step of the flow chart, which generates the basic block module, will be discussed soon in this section. The third step shown in the flow chart is to repeat the building block, or the small grid module as mentioned above, for every slot pitch in a two-pole pitch span in the MLA to complete a tetrahedral element grid in one half length of the machine. Since the modules in adjacent slots must share the nodes on their interface, some programming treatment methods are employed to avoid the occurance of duplicate nodes in this module repeating

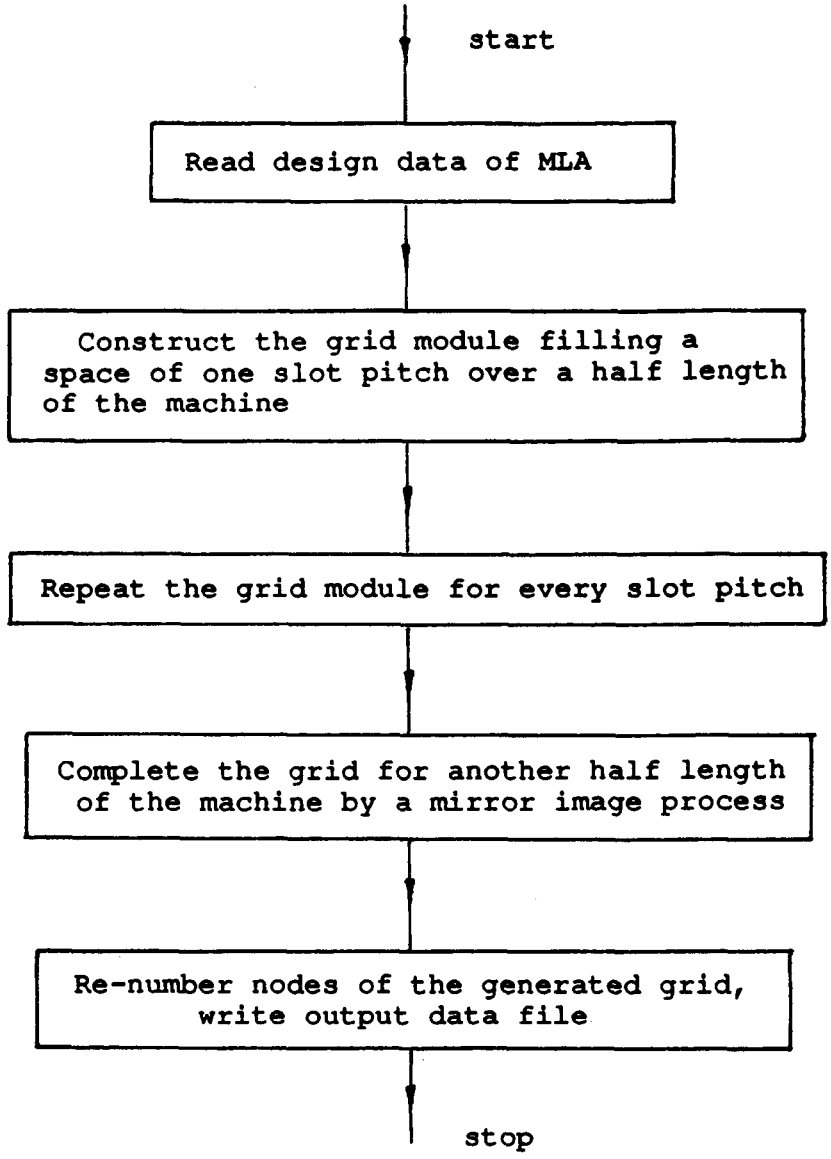

Figure 4.13 Flow Chart for Stator Grid Generation

process.

Besides, the material number for the armature coil part in the grid module is subject to change during this module-repeating work stage. This is because armature coils in different slots, or in the same slot but different layers, may belong to a different phase in the armature winding. Hence, they have to be identified from each other with a numbering sequence so that the correct phase current distribution can be assigned later to perform magnetic filed computations under various machine load conditions.

The next step of the flow chart in Figure 4.13 is to mirror image the grid which has been generated by the previous steps, to form the stator grid corresponding to the given machine geometry. The last step of the flow chart is renumbering all generated nodes for the convenience of the stator-rotor grids connection to form the global grid. The last step is being presently developed by these investigators.

The construction work for the basic building block module of the stator grid is presented in a picture shown in Figure 4.14. The module is generated by combining further small work blocks, *Block I*, *Block II*, and *Block III*, as shown in Figure 4.14. Instead of building these work blocks in terms of different machine parts, they are formed according to consideration of the geometry features. This means that each chosen block has simple geometry structure so that the grid inside the block can be built up mainly by triangular prism super-elements. Blocks *I* and *III*, as well as Block *I* and *II*, are connected together directly because they can share common interfaces, respectively. However, *Block II* can not be connected directly to either *Block III* or to the cylindrical surface in the middle of the main airgap, which is the bottom surface shown in Figure 4.14. The reason for this is

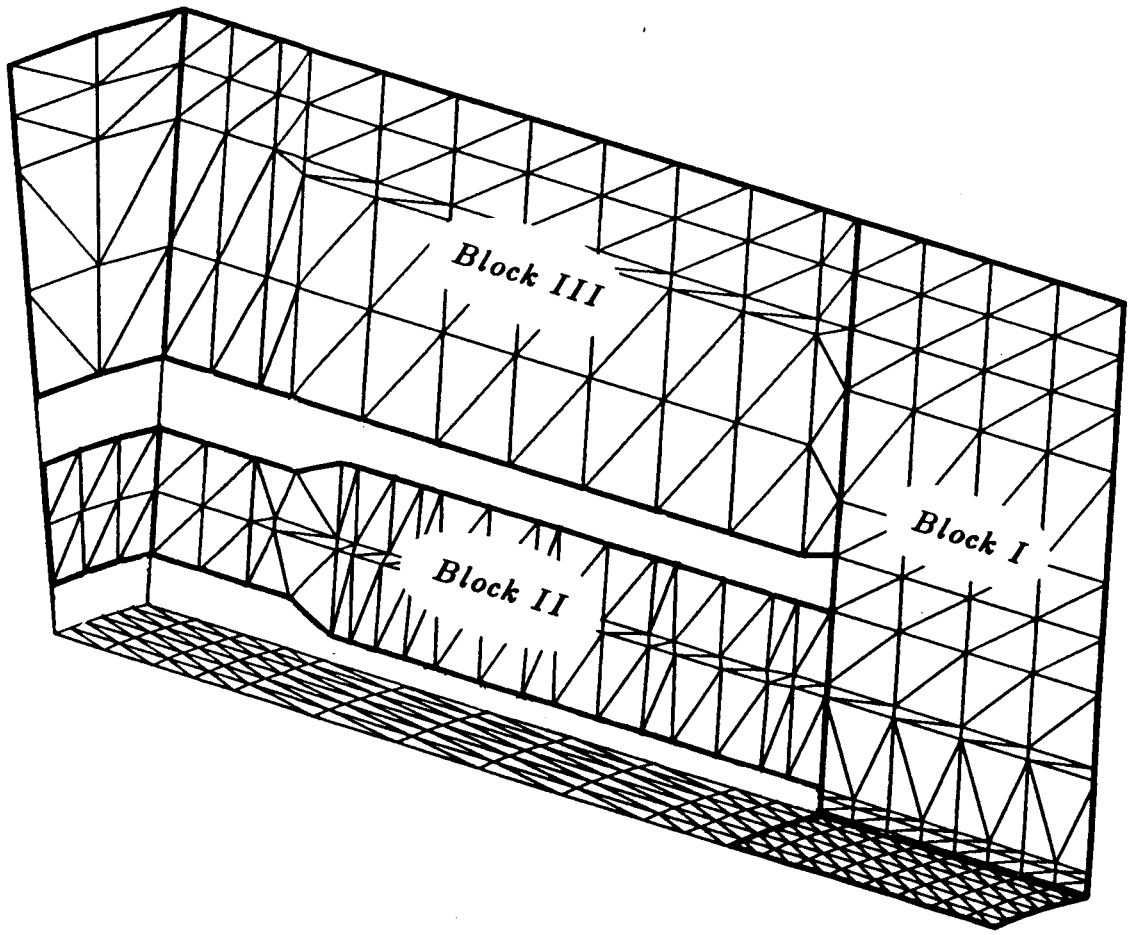

Figure 4.14 Work Blocks of the Grid Module for Stator FE Grid

that the grid topology of *Block II* may change due to different designs of the armature coil pitch, which may be required by further design modification studies at later stages of this research project. Thus, the filling technique which has been described in Section 3.0 of this report, is used to complete the tetrahedral grid between *Block II* and *Block III*, that joins the two blocks in the stator grid module, as well as the grid between *Block II* and the cylindrical surface at the middle of the main airgap.

The tetrahedral grid filling *Block II*, shown in Figure 4.14, is the most complicated task in the stator finite element grid generation. This block contains complex geometry of the end turn region of the armature winding, and the dimensions and topological geometry will change when the design of the armature slot pitch varies. In order to tackle these difficulties, a further partition for *Block II* was made, which allows one to build up grids in each small subblock, in Figure 4.15, then connect them together to complete the grid filling the geometry of *Block II*.

Subblock, A, of *Block II* in Figure 4.15 is the geometry portion where the upper bar and the lower bar of the armature winding exit out of the slot and begin to bend in opposite directions. Subblock, B_1, in Figure 4.15 is the region in which the upper coil bar and the lower coil bar cross each other. It must be understood that the upper bar and the lower bar in Subblock, B_1, belong to the portions of two different coils embeded in the slots adjacent to the slot containing *Block II*. Subblock, B_2, in Figure 4.15 has the same geometric nature and grid topology as those of subblock, B_1. If the armature coil pitch increases, more subblocks than B_1 and B_2, with an identical tetrahedral element grid, will have to be used. This is because the greater the armature coil pitch, the more upper coil bars and lower coil bars corss each other in the end turn region. Subblock, C, in Figure 4.15 contains

the U-turn of the end turn part of the armature coil, which means that in the region of Subblock, C, the coil bar bends in the radial direction to make a U-turn from the upper layer to the lower layer, or vise versa. Subblock, D, in Figre 4.15 includes the free space between the coil bar and the endbell, as well as the endbell part within *Block II*.

Figure 4.16 represents the generated grid filling *Block II* and two sets of triangles on the top surface and the bottom surface of the block. The top surface triangles are used for filling the tetrahedral element grid in the gap beteen *Block II* and *Block III*, and the bottom surface triangles in Figure 4.16 are used for filling the tetrahedral element grid in the gap between *Block II* and the mid-airgap surface, as is shown previously in Figure 4.14.

It should be pointed out that the summation of the volumes of all the tetrahedral finite elements constituting the present stator grid, based on computer obtained numerical values, was found to be 62.8333 cubic inch (in^3). Meanwhile, a simple hand calculation of the same cylindrical shell volume of the stator grid yields a value of 62.9388 cubic inch (in^3). This close agreement between the two volume results confirms the very good accuracy of the stator's FE grid discretization. The slight discrepancy between the two numbers is to be expected, and is due to the fact that in the finite element discretization (or tetrahedral) faces are planes, while the actual volume has cylindrical type surfaces. This is somewhat similar in nature to the situation in two dimentional grids when circles are approximated by a series of cords instead of arcs. Further explanation of the stator grid will be provided during an oral presentation which is anticipated to take place at NASA Lewis Research Center in May of 1988, as well as in future reports. In the next section the rotor grid is briefly discussed.

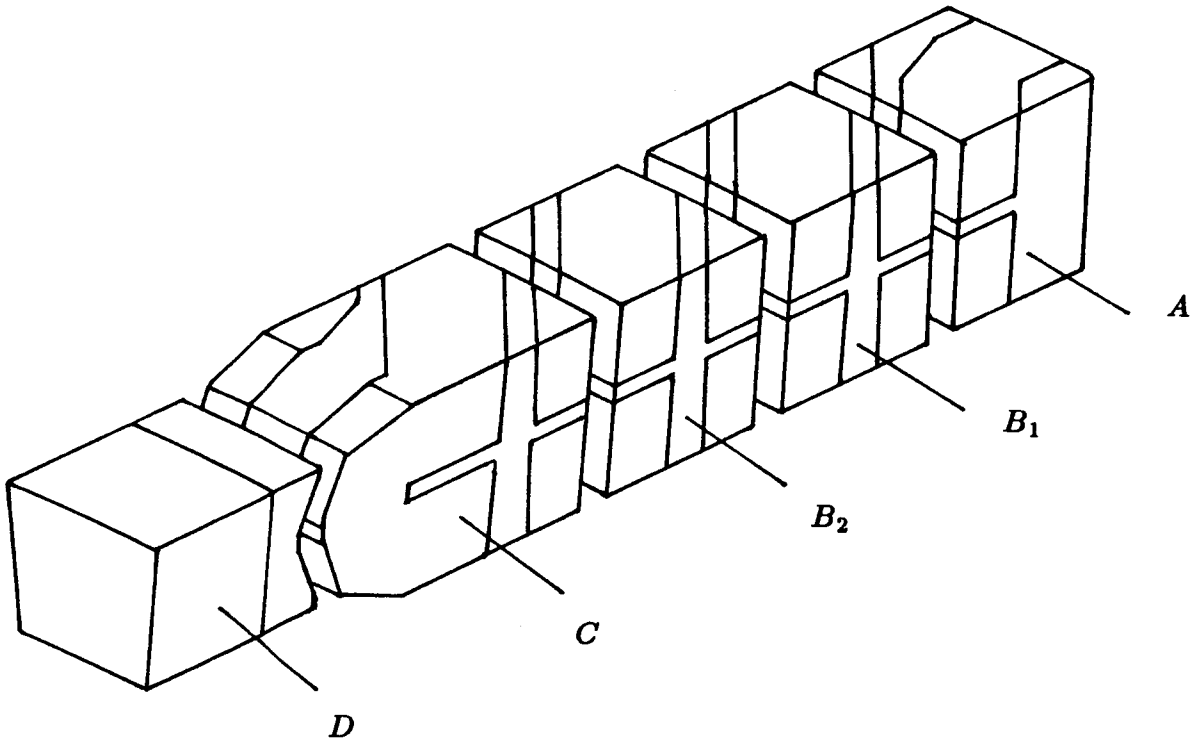

Figure 4.15 End Turn Grid Construction - Subblocks

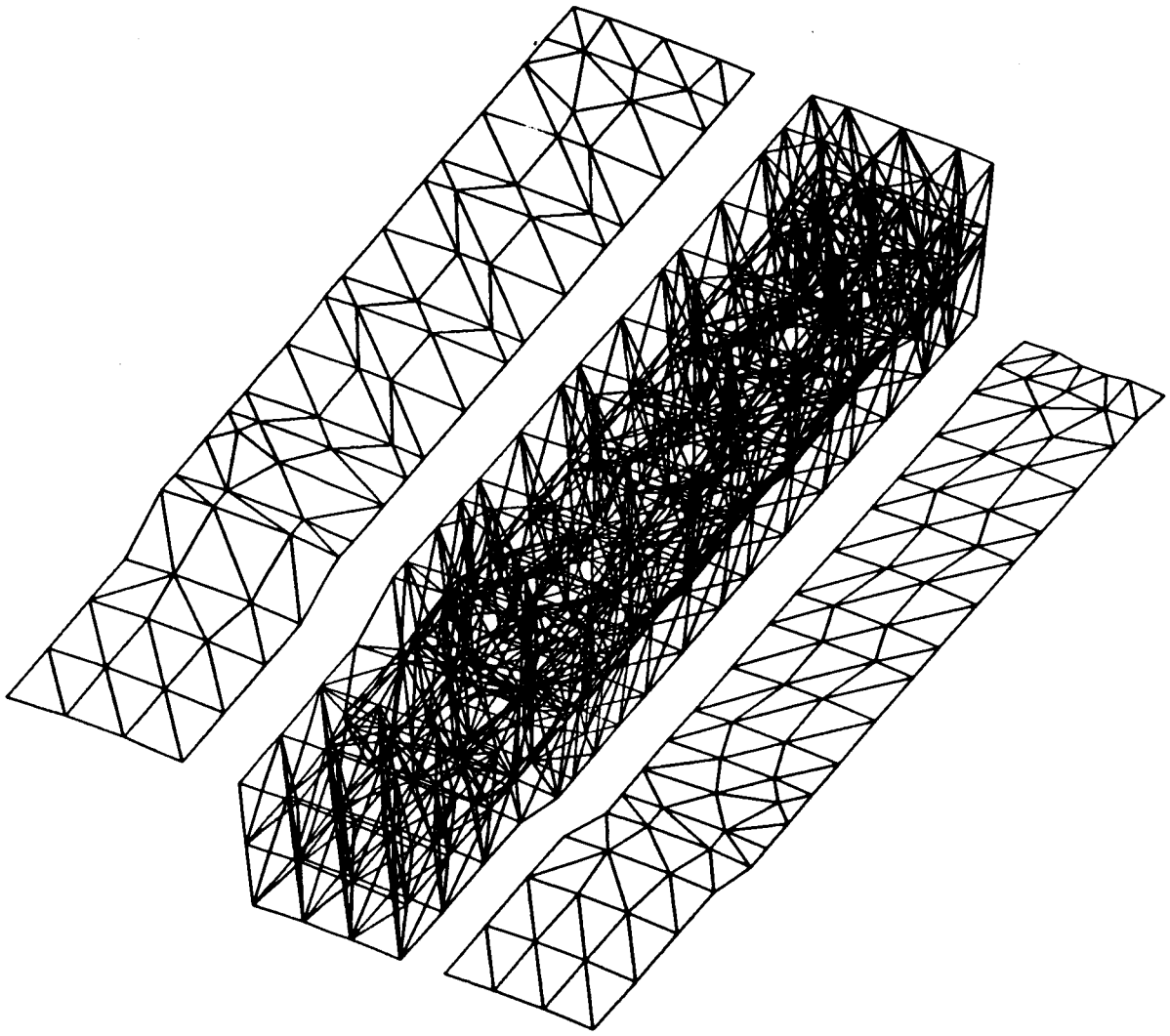

Figure 4.16 Block II - Tetrahedral FE Grid Filling

5.0 ROTOR FINITE ELEMENT GRID GEOMETRY

The finite element grid filling the geometry of the rotor is currently being developed by these investigators. As explained in Section 4.0, the volumetric region of the rotor grid is a cylindrical shell, which contains the rotor, half of the cylindrical shell of the main airgap, the axiliary airgap, and a portion of the endbell. Since this rotor grid must be connected to the stator grid, as discussed earlier in Section 4.0, the outer cylindrical surface of the rotor grid should have the same discretization as that on the inner cylindrical surface of the stator grid, such that the rotor grid and the stator grid can be "stiched" together by sharing the nodes and surface triangles on their cylindrical interface (surface).

According to the symmetry nature of the rotor geometry, a grid module which fills one octant of the volumetric region of the rotor grid is being generated at first. Such an octant is shown in the first octant of the 3-D space as displayed in Figure 5.1. Then a conterpart of this module, which is located in the second octant of Figure 5.1, is being generated by mirror imaging the grid module in the first octant, with respect to the YOZ referece plane. The remaining portion of the rotor grid, which is in the fifth and the sixth octants of the 3-D space, will have been completed by rotating and mirror imaging the grid modules in the first and the second octants. Namely, this means that one rotates the grid module in the first octant by (90) mechanical degrees around the Z-axis, then mirror images it with respect to the XOY reference plane to form the grid in the sixth octant. Similarly, one rotates the grid module in the second octant by (-90) mechanical degrees around the Z-axis, then mirror images it with respect to the XOY reference plane to form the grid in the fifth octant of the 3-D space. The inside geometry

of the rotor is a very complicated one. A series of cross-sectional drawings has to be used to explain the inner details of this complex geometry. Accordingly, the volumetric octant of the grid module is being cut into pieces, or disks, by a number of cross-sectional planes, then each of these cross-sectional surfaces is separatly discretized into triangels. Finally, tetrahedral finite elements are filled into the pieces, or disks, between these cross-sectional surfaces to complete the rotor grid. The filling technique discussed in earlier sections of this report will be used as a main tool for the generation of the rotor grid. Details of this part of the work and resulting rotor grid will be shown in future reports.

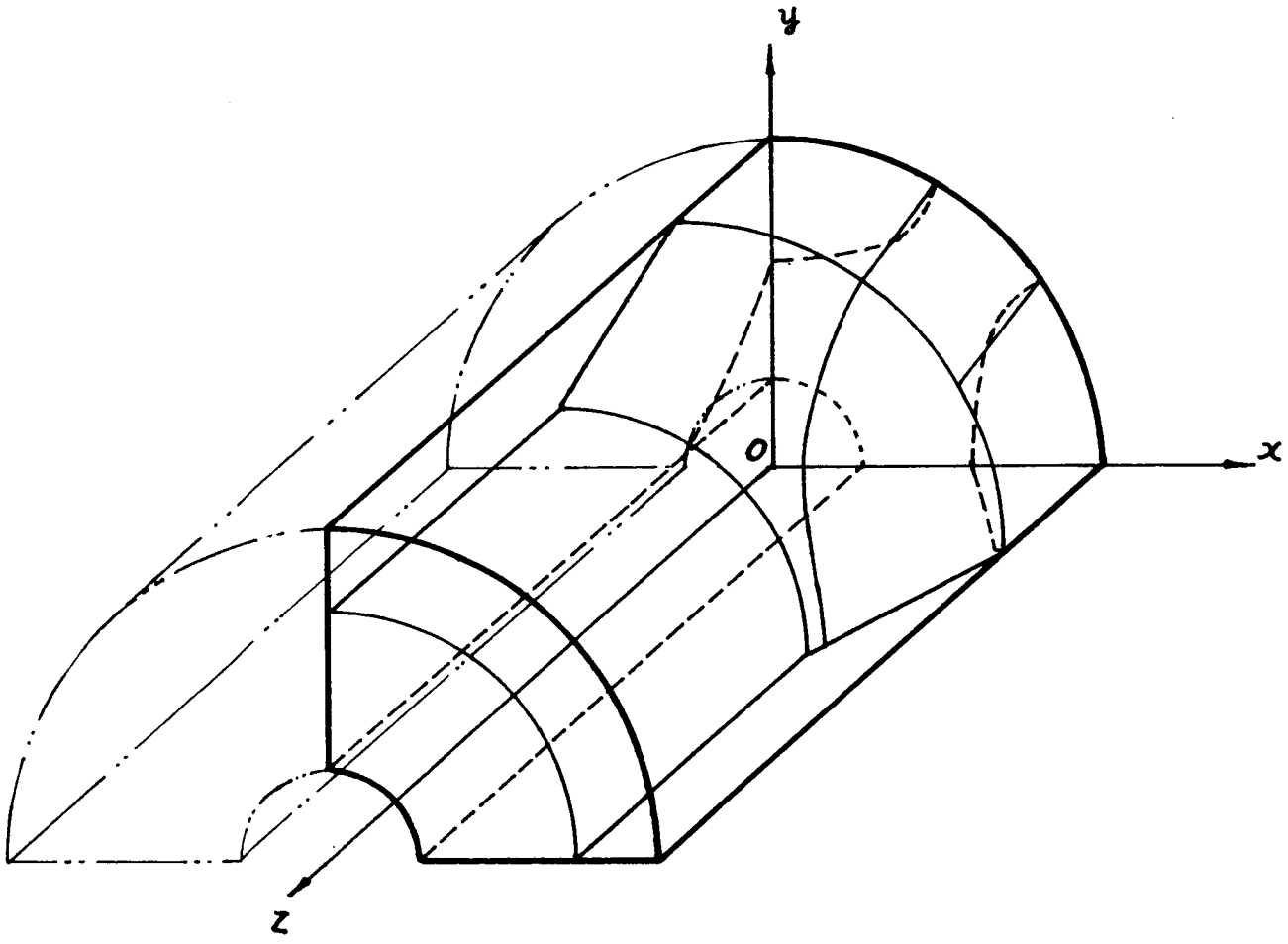

Fig 5.1 Initial Development of Rotor FE Grid Module and Discretization

6.0 IMMEDIATE FORTHCOMING EFFORTS

Over the period of the next 6 months, a very brief summary of the tasks ahead can be listed as follows:

(1) Complete the FE discretization of the rotor portion of the global FE grid of the MLA Class of machines. That is, complete the rotor FE grid.

(2) Assemble the rotor and stator FE grids to form the global FE grid, and recheck all geometries and data of the example 14.3 kVA MLA, and experiment with numerous rotor positions relative to the stator to assure the generality of the FE discretization for magnetic field computation purposes.

(3) Experiment with geometric parameter change in various parts of windings, magnetic cores, and airgaps to ascertain the generality of the FE discretization for purposes of studying various design options.

(4) Attempt a preliminary 3-D FE magnetic field solution at no-load, and without inclusion of magnetic nonlinearities. That is, obtain the open-circuit airgap line characteristics of the example 14.3 kVA MLA.

(5) Attempt a saturated nonlinear magnetic field solution of the MLA at several field excitations near and above rated open circuit voltage. Compare results with previous or new data on the open-circuit no-load characteristic of the example 14.3 kVA MLA.

(6) If steps (1) through (5) are complete, proceed to short circuit, zero power factor, and other load cases. Further steps will be outlined in the second six month progress report.

7.0 CONCLUSIONS

The investigation is proceeding as scheduled at the expected pace. The stator finite element grid of the MLA class of alternators is now complete, as given earlier in this report. The rotor FE grid is presently being developed. Both stator and rotor FE grids, which form the global MLA-FE grid are expected to be reported on in an oral presentation, which is expected to take place at the NASA-Lewis Research Center at a date in May 1988 to be agreed upon with NASA Lewis personnel.

8.0 REFRENCES

[1] Demerdash, N.A., "Computer-Aided Modeling and Prediction of Performance of the Modified Lundell Class of Alternators in Space Station Solar Dynamic Power Systems," Research Proposal submitted to NASA, April 1987.

[2] Repas, D.S., and Edkin, R.A., "Performance of Characteristics of a 14.3-Kilovolt-Ampere Modified Lundell Alternator for 1200 Hertz Brayton-Cycle Space Power System," *NASA Reprot*; NASA-TN-5405, sept. 1969.

[3] Demerdash, N.A., Nehl, T.W., and Fouad, F.A., "Finite Element Formulation and Analysis of Three Dimensional Magnetic Field Problems," *IEEE Transactions on Magnetics*, Vol. MAG-16, No. 5, 1980, pp. 1092-1094.

[4] Demerdash, N.A., Nehl, T.W., Fouad, F.A., and Mohammed, O.A., "Three Dimensional Finite Element Vector Potential Formulation of Magnetic Fields in Electrical Apparatus," *IEEE Transactions on Power Apparatus and Systems*, Vol. PAS-100, No. 8, August 1981, pp. 4104-4111.

[5] Demerdash, N.A., Nehl, T.W., Mohammed, O.A., and Fouad, F.A., "Experimental Verification and Application of the Three Dimensional Finite Element Magnetic Vector Potential Method in Electrical Apparatus," *IEEE Transactions on Power Apparatus and Systems*, Vol. PAS-100, No. 8, August 1981, pp. 4112-4122.

[6] Mohammed, O.A., Demerdash, N.A., and Nehl, T.W., "Nonlinear Vector Potential Formulation and Experimental Verification of Newton-Raphson Solution of Three Dimensional Magnetostatic Fields in Electrical Devices," *IEEE*

Transactions on Energy Conversion, Vol. EC-1, No. 1, 1986, pp. 177-185.